University of Nairobi

School of Engineering

Application of Geospatial Technologies in the Selection of Suitable Geothermal Well Sites: A case study of Eburru Volcanic Complex

BY

Bernard Mageto Omwenga

F56/8079/2017

A project Submitted in partial fulfillment of the requirements for the Degree of Master of Science in Geographic Information Systems in the Department of Geospatial and Space Technology of the University of Nairobi

August 2019

Declaration

I, Bernard Mageto Omwenga, hereby declare that this project is my original work. To the best of my knowledge, the work presented here has not been presented for a project in any other institution of Higher Learning.

…… ……

Name of student Date

……..

Signature

This project has been submitted for review with our approval as University supervisor(s).

…… ……

Name of supervisor Date

…… ……

Name of supervisor Date

DEDICATION

I dedicate this work to my family for their support during the academic journey and in this project. My Wife Christine, daughter Delyne Gabriel as well as friends and colleagues at the work place. May God abundantly bless you.

ACKNOWLEDGMENT

I would like to acknowledge my employer, Kenya Electricity Generation Company (KenGen) for approving my studies. I would also like to acknowledge my supervisor, Mr. P.C. Wakoli for the guidance in the project writing. Special thanks to my family for their support. Ultimately, the Almighty God for strength and protection during my study period.

ABSTRACT

The study applied geospatial techniques to establish favorable areas for geothermal well siting in the Eburru Volcanic Area, Nakuru County. The study's main objective was to apply remote sensing and Geographic Information Systems (GIS) to select suitable sites for geothermal wells. The specific objectives of the study involved the use of GIS multi-criteria evaluation and weighting of the distinct data layers (factor maps) for development of a final geothermal well suitability map. A suitability map was created by weighting and overlaying geothermal factors from three disciplines, namely: geology (faults, eruption centers, and dykes), geochemistry (altered grounds, fumaroles, hot grounds) and thermal factors (satellite land surface temperature, heat loss measurements). Environmental constraints such as built up areas, forest cover and riparian area (lake) were buffered, overlaid and filtered over the combined suitability map to establish a final suitability model. The methodology employed a multi-criteria approach using weighted overlay analysis, Boolean logic methods that supports conventional field based well site selection methods such as geology, geophysics and geochemistry. The results of the final suitability map was a classification of the study area into three primary regions namely; most suitable area, moderately suitable area and the least suitable area. Areas near Eburru trading centre, Thome (Northern region) and Badlands rift axis were found to be most suitable. The central and western regions of the study area were deemed to be moderately suitable. North Eastern zones (near Gilgil and Kikopey towns were found to be the least suitable. The study recommended the adoption of the technique in well siting activities.

Table of contents

Declaration i

ABSTRACT iv

Table of contents v

LIST OF FIGURES ix

List of Tables x

Nomenclature xi

CHAPTER ONE 1

1 INTRODUCTION 1

1.1 Background Information 1

1.2 Problem statement 2

1.3 Study objectives 2

1.3.1 General objective 2

1.3.2 Specific objectives 2

1.4 Justification of the study 2

1.5 Scope of study 3

1.6 Organization structure of the Report 3

CHAPTER TWO 4

2 LITERATURE REVIEW 4

2.1 Geothermal Energy Resource 4

2.1.1 Geothermal resources in Kenya 5

2.2 Geothermal resource exploration 6

2.2.1 Field based geothermal exploration approaches 7

2.2.2 GIS in geothermal exploration 8

2.2.3 Remote sensing in geothermal exploration 8

2.3 Previous studies 10
2.4 Geothermal Factors 11
2.4.1 Geological Factors 11
a. Faults, fractures and open fissures 11
b. Craters and caldera (Eruption centers) 12
c. Geothermal index mineral indicators 12
2.4.2 Geochemical Factors 13
a. Fumarole activity 13
b. Hydrothermal alteration zones 13
2.4.3 Thermal Factors 14
a. Heat loss measurements 14
b. Satellite Land surface Temperature measurements 14
2.5 Geothermal well site suitability selection process 17
2.5.1 Problem definition 18
2.5.2 Definition of Constraints 18
2.5.3 Definition of criteria 18
2.5.4 Standardization of Criteria 19
2.5.5 Criteria weighting 19
2.5.6 Aggregation of the geothermal well selection factors 19
CHAPTER THREE 20
3 MATERIALS AND METHODS 20
3.1 Study area 20
3.2 Data types and sources 21
3.3 Procedure 21
3.3.1 Data collection methods 21

3.3.2 Re-projection and transformation 21
3.3.3 Image pre-processing and enhancement 21
3.3.4 Analysis 22
3.3.5 Information presentation and interpretation 22
3.4 Overview of the study methods 24
3.4.1 Remote sensing techniques 24
a. Band composite and Image Pan sharpening 24
3.4.2 GIS techniques 25
a. Digitization and conversion of vector to raster 25
b. Euclidian distance analysis 26
a. Reclassification of the distance maps 29
b. Spatial interpolation and Land surface temperature estimation by NDVI threshold . 31
c. Weighted Overlay Analysis (WOA) 32
3.5 Individual suitability determination Criteria 33
3.5.1 Constraint Criteria 33
3.5.2 Geological Suitability 35
3.5.3 Geochemical suitability map 36
3.5.4 Thermal suitability map 38
3.5.5 Combined Geothermal suitability map 39
3.6 The Existing Eburru suitability maps 40
CHAPTER FOUR 43
4 RESULTS AND DISCUSSION 43
4.1 Criteria weights 43
4.2 Final Suitability map 44

4.3 Comparison between the final geothermal suitability map and existing Eburru suitability map 46

4.3.1 Discussion 47

CHAPTER FIVE 48

5 CONCLUSIONS AND RECOMMENDATIONS 48

5.1 Conclusion 48

5.2 Recommendations 49

REFERENCES 50

Appendix 1: Heat Loss survey measurements of the study area 57

Appendix 2: Location of Sampled wells 60

Appendix 3: Fumarole temperatures 61

Appendix 3: User Requirement Analysis 62

LIST OF FIGURES

Figure 2.1: Simple representation of an ideal geothermal system (Dickson & Fanelli, 2004)..... 4
Figure 2.2: Geothermal prospects in the Kenyan rift (Omenda, 2013) 5
Figure 3.1: Location of the study area 20
Figure 3.2: Schematic workflow of the data processing..... 22
Figure 3.3: Flow diagram showing steps used to identify suitable sites for geothermal wells..... 23
Figure 3.4: True color composite map of Eburru area..... 24
Figure 3.5: False color composite map of Eburru area..... 25
Figure 3.6: Digitized map of study area..... 26
Figure 3.7: Geological distance factor maps (Faults and dykes)..... 27
Figure 3.8: Geological factor distance map of the study area (Eruption centers)..... 27
Figure 3.9: Geochemical factor distance map of the study area (fumaroles and altered grounds)28
Figure 3.10: Geochemical factor distance Map of study area (Hot grounds)..... 28
Figure 3.11: Eruption Centers reclassified map of the study area 29
Figure 3.12: Dykes and faults reclassified maps of study area..... 30
Figure 3.13: Fumaroles and hot grounds reclassified maps of the study area 30
Figure 3.14: Interpolated heat loss survey map of study area..... 31
Figure 3.15: Land surface temperature map of study area..... 32
Figure 3.16: Weighted overlay analysis process..... 32
Figure 3.17: Restricted zones of the study area 34
Figure 3.18: The constraint map 34
Figure 3.19: Map showing the Geological Suitability of the study area 36
Figure 3.20: Map showing the geochemical Suitability of the study area..... 38
Figure 3.21: Thermal suitability map..... 39
Figure 3.22: Combined suitability map 40
Figure 3.23: Map showing the recommended drilling sites (Varet, 2017) 41
Figure 3.24: Suitability map of the study area (KenGen, 2018). 42
Figure 4.1: Final suitability map of the study area 44

List of Tables

Table 3.1: Data sources for the study 21
Table 3.2: Color codes for suitability ranking 33
Table 3.3: Selected constraints for the study area 33
Table 3.4: Area of the restricted zones 35
Table 3.5: Classification of faults and influence on geothermal activity (Yousefi et al., 2007) 35
Table 3.6: Classification of eruption centers and influence on geothermal activity(Yousefi et al., 2007) 35
Table 3.7: Classification of dykes and influence on geothermal activity (Yousefi et al., 2007) 36
Table 3.8: Classification of fumaroles and influence on geothermal activity (Yousefi et al., 2007) 37
Table 3.9: Classification of altered grounds and influence on geothermal activity (Yousefi et al., 2007) 37
Table 3.10: Classification of Hot grounds and influence on geothermal activity (Yousefi et al., 2007) 37
Table 3.11: Classification of Temperature and influence on geothermal activity (Yousefi et al., 2007) 38
Table 4.1: Weighted index table for geological features (User satisfaction survey) 43
Table 4.2: Weighted index table for geochemical features (User satisfaction survey) 43
Table 4.3: Weighted index table for surface temperature (User specification survey) 43
Table 4.4: Weighted overlay analysis procedure ((Mayfield, 2016) 44
Table 4.5: Suitable areas for geothermal well siting in the study area 45
Table 4.6: Area of coverage combined suitability classes 45
Table 4.7: Comparison between existing and new suitability map 46

Nomenclature

ASCAT-Advanced Scatterometer

ASTER- Advanced Spaceborne Thermal Emission and Reflection Radiometer

AVIRIS-Airborne Visible Infrared Imaging Spectrometer

Bgl-Below Ground Level

DEM-Digital Elevation Model

ERC-Electricity Regulation Commission

ETM +-Enhanced Thematic Mapper plus

EW-Eburru Well

GIS-Geographic Information Systems

KenGen-Kenya Electricity Generation Company

LST-Land Surface Temperature

MW - Megawatts of energy

OLI-Operational Land Imager

OW-Olkaria Well

OWA-Overlay Average Weighted

PALSAR-Phased Array type L-band Synthetic Aperture Radar

PCA-Principal Component Analysis

SEBASS-SeaBass

SWIR-Short Wavelength Infrared

TIR-Thermal Infrared

UAV- Unmanned Aerial System

USD-United States Dollar

VNIR-Visible and Near Infrared

WOA-Weighted Overlay analysis

WLC-Weighted Linear Combination

CHAPTER ONE

1 INTRODUCTION

1.1 Background Information

Geothermal energy is derived from the heat contained in the Earth (Noorollahi et al., 2015). It originates from the Earth's crust as a result of radioactive decay of subsurface materials. It is considered cost-effective, reliable, sustainable and environmentally friendly (Glassley, 2014) and therefore offers a renewable and sustainable source of energy. As result, it has been considered viable reliable alternative energy as compared to hydro sources that are constantly affected by unpredictable weather patterns and climate change. Other indirect applications of geothermal energy include: using hot springs for bathing, cooking, drying, and refrigeration among others.

The conventional geothermal well site selection methods is done using multi-disciplinary field investigations such as geological mapping, monitoring of geothermometers, manifestation alteration zones identification and geophysical measurements. These field-based techniques are relatively costly, time-consuming and limited by accessibility and in some instances, adverse weather conditions. Remote sensing and GIS are alternative well site selection methods useful for developing decision support models in geothermal resources development projects. They are relatively cost-effective methods that complement the traditional field-based well siting techniques. Remote sensing can be used to pinpoint geothermal anomalies, thereby identifying suitable zones for geothermal wells. The geothermal anomalies are temperature related observed as surface expressions on the earth's surface such as fumaroles, hot springs, geysers, mud pools, and altered grounds, open faults, fractures, eruption centers, dykes among others. Satellite land surface temperature measurements can also be used to identify geothermal anomalous zones. For this study, the evidence features have been classified as follow: Geological (faults, dykes, eruption centers), geochemical (fumaroles, altered grounds, hot grounds) and thermal (land surface temperature, heat loss surveys). Upon recognizing geothermal anomalous areas, deep wells are drilled in these areas to generate steam which is thereafter harnessed for electricity generation. The drilling exercise is usually risky and expensive. For instance, a 3.5km deep well costs about 5.8m USD according to estimates by Kipsang (2015). It is therefore important that precision and accuracy be taken to consideration when siting these wells.

1.2 Problem statement

Traditional geothermal site selection comprises multi-disciplinary field approach involving the integration of various surface exploration methods such as geological, geochemical, geophysical and environmental baseline surveys. These methods are costly, cumbersome and usually hindered by terrain ruggedness, inaccessibility and adverse weather conditions. Knowledge gaps may arise in the inaccessible and unexplored areas. In addition, the aforementioned challenges lengthens geothermal resource exploration duration which in effect increases the overall cost of the geothermal resource development project.

The research therefore opted to use geographical information systems multi-criteria analysis and remote sensing image analysis techniques to provide an alternative solution to the stated problem.

1.3 Study objectives

1.3.1 General objective

The general objective of the study is to apply remote sensing and GIS techniques to select suitable sites for geothermal wells in Eburru Volcanic area, Nakuru County (Kenya).

1.3.2 Specific objectives

i. To identify the criteria for selecting suitable sites for geothermal wells.
ii. To establish the relative weights of the identified criteria.
iii. To perform a multi-criteria evaluation analysis to generate the final suitability.
iv. To compare the final suitability map with the existing maps generated using different geoscientific approaches.

1.4 Justification of the study

Investors in the energy sector require organized datasets to decide if the area fits their expectation before deciding to finance a project. A geothermal suitability map is part of the dataset. By understanding the precise location of geothermal manifestation features in the area of study, stakeholders in the energy sector will be confident when investing their resources in the geothermal sector. The study results will also be used to infill the knowledge gaps that are posed by conventional geoscientific surface exploration methods. The GIS-based decision support will also be used by geothermal planners, resource managers, for site selection to make optimal choices for locating, conducting, and sustaining restoration project sites

1.5 Scope of study

The study focused on establishing suitable geothermal well potential areas using remote sensing image analysis techniques and GIS platform multi-criteria analysis. This was in an attempt to develop geothermal suitable resource prospect zones at the Eburru Volcanic area (Rift Valley), Kenya. The study was conducted in five phases namely: desktop studies, reconnaissance, fieldwork, data analysis, and interpretation and presentation. Reconnaissance was used to familiarize with the study area, identify challenges and seek permission from the relevant authorities before the commencement of actual fieldwork. Thereafter, actual field work was carried out for ten days followed by data analysis, interpretation and presentation of results.

1.6 Organization structure of the Report

This report consists of five chapters starting with introduction, which highlights the research background, problem statement and objectives, justification, and the scope of the research.

Chapter two discusses detailed review of the geothermal systems, exploration and the various geospatial techniques of well site selection. Chapter three deliberates the various methods, materials used for the study. Chapter four outlines and discusses the study's findings based on the multi-criteria approach. Chapter five outlines the study's conclusions and recommendations.

CHAPTER TWO

2 LITERATURE REVIEW

2.1 Geothermal Energy Resource

Geothermal systems occur in regions of anomalously high crustal heat flow that may be related to the presence of young igneous bodies or hot rocks located deeper in the crust (Rybach, 1981); (Haselwimmer & Prakash, 2013). The heat from the geothermal reservoir can be extracted and utilized economically for power generation, agricultural purposes, and refrigeration among others. When the heat contained within fluid filling fractures and permeable rocks is sufficiently accessible, it can be exploited for power generation (Haselwimmer & Prakash, 2013).

In areas of high crustal heat flow geothermal power offers an attractive low-carbon alternative to traditional fossil-fuel based energy and as such, there is increasing interest in the exploration and development of new geothermal resources such as in the Great Basin of the western United States (Haselwimmer & Prakash, 2013). Studying surface geothermal activity and heat loss associated with magmatic related systems is important for monitoring of subsurface igneous activity and to conserve geothermal systems that are of cultural significance or are economically important tourism destinations (Bromley & Graham, 2010). Figure 2.1 is a perfect pictorial representation of a geothermal system.

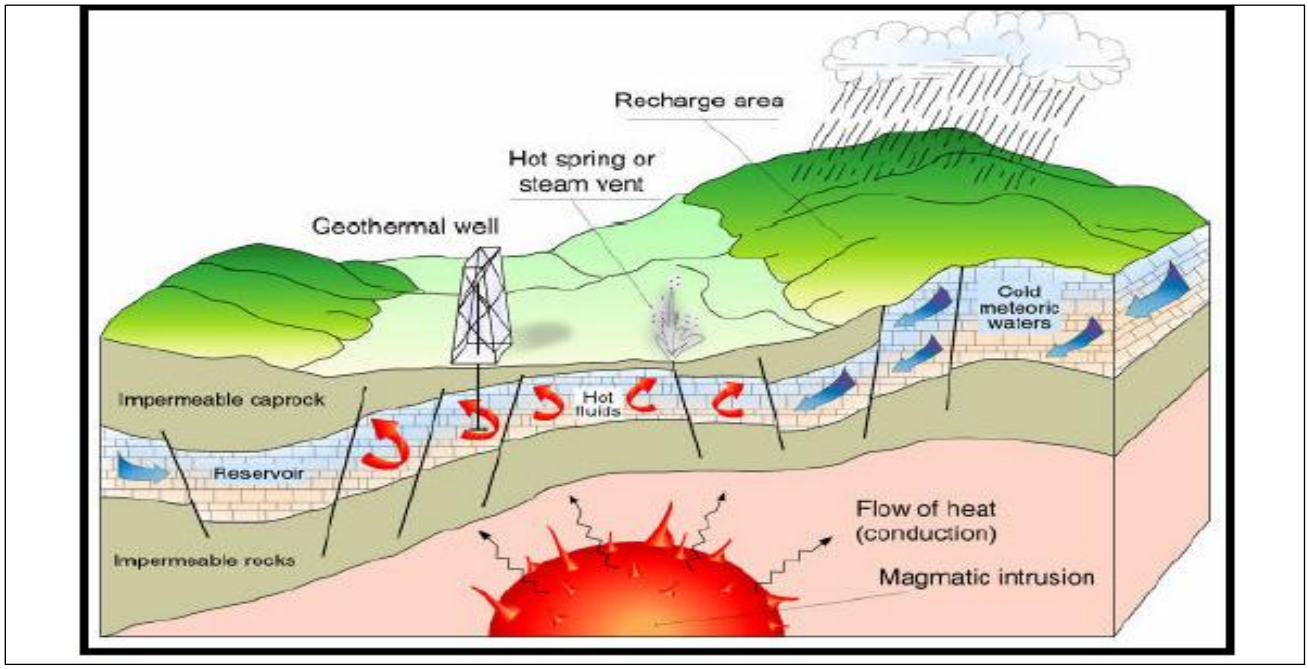

Figure 2.1: Simple representation of an ideal geothermal system (Dickson & Fanelli, 2004)

Geothermal energy development is fundamentally a chronological and a methodical process of exploring productive sites with the ultimate aim of geothermal power production. The development phases begin with reconnaissance and exploration, pre-feasibility, feasibility and finally power plant construction (Ochieng, 2013).

2.1.1 Geothermal resources in Kenya

Kenya is endowed with significant geothermal resources as part of the East African Rift System (Macharia et al., 2017). It is one of the leading countries globally with significant geothermal resources with rich geothermal potential sites being along the Rift Valley (Mibei, 2012). The geothermal resources within the Kenyan Rift are found in abundance in the following areas: Olkaria, Menengai, Eburru, Baringo, Korosi, Paka, Silali, Emuruangogolak and Barrier (Figure 2.2). However, prospects such as Homa Hills, Chyullu Hills and Mwanyamala are located outside the Rift Valley. The estimated potential of geothermal energy of the Kenyan Rift lies between 7,000 MW to 10,000 MW spread over 14 prospective sites (ERC, 2012).

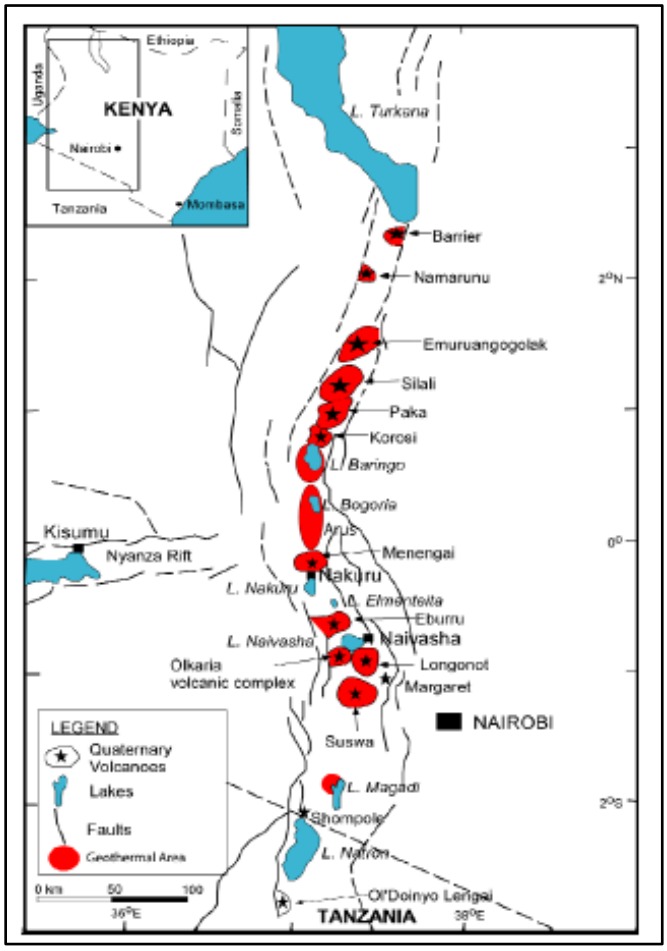

Figure 2.2: Geothermal prospects in the Kenyan rift (Omenda, 2013)

2.2 Geothermal resource exploration

Geothermal exploration is usually carried out in order to locate a geothermal system from which the energy can be utilized for the economic purpose. The common surface geothermal exploration techniques include Geological, geochemical studies, and a variety of geophysical techniques including gravity, magnetic seismic and electrical resistivity. Surface exploration is usually done to detect the surface anomalies that occur as a result of the presence of aforementioned surface manifestation features. Proper surface exploration increases the likelihood of realization with subsequent drilling and development (Árnason, Vilhjálmsson, & Björnsdóttir, 2007), thereby reducing the risks and losses associated with the project.

The main objectives of geothermal exploration according to Noorollahi (2005) are outlined as follow:

- To ascertain geothermal phenomena.
- To determine that a useful geothermal production field exists.
- To evaluate the size of the resource.
- To determine the type of geothermal field.
- To pinpoint productive zones.
- To determine the heat content of the fluids that will be discharged by the wells.
- To compile a body of basic data against which the results of future monitoring can be viewed.
- To determine the pre-exploitation values of environmentally sensitive parameters.
- To acquire knowledge of any characteristics that might cause problems during field development.

Exploration of geothermal resources in Kenya started in the 1960s with the drilling of two geothermal wells in Olkaria (OW-X1 and OW-X2). More geological and geophysical studies were carried out in Lake Bogoria, Olkaria and Lake Baringo areas in the1970s. Additional wells were thereafter drilled to prove enough steam for the generation of electricity and in June 1981, the first 15 MW generating unit was commissioned at Olkaria geothermal field. The second 15 MW unit was commissioned in November 1982 and the third unit in March 1985 which increased the total generation to 45 MW (Omenda, 2013). The Kenya Electricity Generating Company (KenGen) Ltd., then Kenya Power Company (KPC) Ltd carried out detailed surface exploration studies at the Eburru geothermal field between 1985 and 1990. Six (6) exploration wells to an average depth of 2.5 km were drilled during this period. Out of the six (6) wells drilled, only three wells (EW-

01, EW-04 and EW-06) discharged (KENGEN, 2018). However, wells EW-04 and EW-06 yielded a higher water phase as opposed to steam phase during discharge and, were consequently shut down. Currently, only well EW-01 which sustained discharge is generating 2.4 MW with a maximum bottom-hole temperature of 278 °C (KENGEN, 2018).

Exploration activities in other areas is still ongoing in most prospect areas. This is in line with the government's target to attain 5000 MW geothermal capacity by the year 2030.

2.2.1 Field based geothermal exploration approaches

The general principle of the process is to work from whole to part, and from the surface to the subsurface (Mwaura, 2018). The following are the notable field based techniques for geothermal resource exploration:

Geochemical exploration: Samples are taken from existing hot springs and analyzed. The results allow estimates to be made regarding the temperature of the fluid at the depth of the reservoir and an estimation of the fluid's origin and recharge within the geothermal reservoir, thereby indicating the degree of permeability within the reservoir rock structure.

Geological exploration: Samples of rocks, sediments, and lava are taken either from the surface or obtained by core drilling to disclose the type of heat source and to estimate its location and potential.

Geophysical exploration: Geophysical technologies provide indications of the events happening in the subsurface. The techniques also provide indications of the subsurface geology structure and the best drilling procedure that would bring hot water to the surface from the geothermal aquifer.

Heat Loss surveys: This is done by boring boreholes, usually less than 500 meters deep and less than 6 inches in diameter, drilled to measure the increase in temperature with depth. The standard temperature gradient worldwide is around 30°C for each additional kilometer in depth, resulting in an average temperature of 90°C at a depth of 3 kilometers. If, in a certain area, the temperature gradient were to increase to 90°C/km, this would result in a temperature of 270°C at a depth of 3 kilometers and would be very promising for geothermal power generation, as long as enough steam could be extracted from the reservoir.

2.2.2 GIS in geothermal exploration

A Geographic Information System is a set of computerized tools (including both hardware and software) for collecting, storing, retrieving, transforming, and displaying spatial data. GIS can be used to define the spatial associations among diverse geothermal evidence layers in an area of interest. GIS functionality, such as vector and raster spatial analysis and overlay, can be employed for structural mapping and analysis using powerful software programs (Abdullah, Nassr, & Ghaleeb, 2013). The success of GIS in sitting problems is attributed to its ability to perform deterministic overlay and buffer operations (Al-Amri & Eldrandaly, 2014). This is usually achieved through organizing, visualization, querying, combining, or analyzing geospatial data. For this study, GIS was used in the following ways:

- Digitization of the original data sets collected from the field in the form of points, poly lines and polygons.
- The spatial analyst relationships allowed the overlaying of remote sensed data with other spatial data layers.
- GIS analyst tools such as proximity analysis (buffering), intersection, distance analysis, reclassification, simple overlay and weighted index overlay were used to build suitability maps.
- Spatial interpolation was used to estimate surface temperature distribution in the study area.
- Replacement of the restricted zones was done using the 'Majority Filter' spatial analyst tool in ArcGIS. This technique replaces the cells in a raster based on the majority of their contiguous neighboring cells.
- The union tool in ArcMap creates a new coverage by overlaying two or more raster coverage for all the involved factors. The output coverage contains the combined rasters and the attributes of all the coverage factors that are input.

2.2.3 Remote sensing in geothermal exploration

The Remote sensing method has been used as a cost-effective tool for geothermal exploration over large areas enabling the succeeding assortment of targets for additional exploration using ground-based studies (Haselwimmer & Prakash, 2013). Remote sensing can be used to assist in the exploration of geothermal prospects by analyzing various images acquired by different sources at respective bands, preferably the thermal infrared band. The basic principle of this technology is to use the 8-14 μm region of the spectral radiant to observe changes in temperature of objects

on the earth's surface. The tone of thermal imagery shows the surface radiance temperature. Remotely sensed thermal infrared (TIR) images have been used for years to detect geothermal activity. High-resolution Thermal Infrared sensors (<5m) are ideal for mapping and monitoring geothermal surface anomalies (Varghese, 2016). Conventional multispectral scanning systems, such as Landsat TM and SPOT XS, record up to 10 spectral bands with bandwidths on the order of 0.10 μm. Hyperspectral scanners are a special type of multispectral scanner that record many tens of bands with bandwidths on the order of 0.01 μm.

Remote sensing can be used for mapping of hydrothermal minerals by monitoring their spectral signatures eye (Lillesand et al. 2015) with reference to the USGS spectral library. Their broad absorption features and spectra are absorbed by the specific remote sensors. These minerals show distinctive spectral reflectance patterns at visible wavelengths and especially at reflected IR wavelengths (Yetkin, 2003).

Remote sensing techniques are useful in the extraction of structural information of the various geological features such as faults, fractures, craters, and calderas geothermal systems. Geological structures can be mapped using high-resolution optical sensors for instance, which offer pixel clarity (Chasia, 2014) but are normally characterized by low spatial resolution.

Digital Elevation Models (DEM) are used for digitizing trace tectonic features and mapping geologically and topographically defined structures in many areas.

The following remote sensing methods were used in the study:

a. Color composite and Pan sharpening

In displaying a color composite image, three primary colors (red, green and blue) are used. The idea behind the color composite technique is to combine the multispectral information with the visible wavelength region, in order to make it visible to the human eye (Lillesand et al. 2015). This enhancement is achieved by combining bands in the visible and in the infrared portions (Mia and Fujimitsu, 2012). With the band combination, rock exposures appeared as brown, vegetated areas as green and built up areas as white. This band combination is applicable for exploratory analysis (Frutuoso, 2015).

A pan sharpened image represents a sensor fusion between the multispectral and panchromatic images which gives the best of both image types, high spectral resolution AND high spatial resolution. Pan sharpening fuse images by decomposing the original images and separately processing the low-frequency and high-frequency part (Zhong et al., 2017). For this study,

panchromatic band 8 of the Landsat 8 OLI with 15m spatial resolution was be used to sharpen a seven band multispectral image (30m resolution) using the component substitution algorithm.

2.3 Previous studies

The application of geospatial technologies (GIS and remote sensing) to establish suitable sites for geothermal energy resources has been studied by a number of researchers.

Velador, Omenda, & Anthony (2003) investigated the structural control of fumarole in the Eburru volcanic complex using Landsat Thematic Mapper and aerial photos. Their study focused on the delineation of faults and their relationship with the surface fumarolic activities. Using GIS spatial analysis tools, they concluded that the N-S normal faults influenced the occurrence of fumaroles and altered zones within the area. They recommended detailed mapping of geological structures in the area using remote sensing and GIS.

Pour, Hashim, & van Genderen (2013) carried a geological analysis coupled with Remote Sensing in the detection of hydrothermally altered rocks and associated structural elements associated with gold mineralization in Bau Gold Mining District, Malaysia. The approach used Enhanced Thematic Mapper plus (ETM+) Hyperion and Phased Array type L-band Synthetic Aperture Radar (PALSAR) to delineate gold mineralization in the area. They concluded that analysis of spectral signatures of minerals associated with gold deposition such as clays, iron oxides and orientation of structural elements coupled by image interpretation of DPC images is essential in the determination of suitable areas for gold exploitation.

Brandmeier et al. (2013) used Advanced Spaceborne Thermal Emission and Reflection Radiometer (ASTER) images to characterize alteration by using hyperspectral field spectrometry data and geochemical analysis in Southern Peru. The research located possible caldera based on alteration patterns of rocks within the study area.

Further studies by van der Meer et al. (2014) combined the aspects of surface deformation, gaseous emission, mineral mapping, heat flux measurements, and geobotany to study the use of geologic remote sensing for geothermal exploration in the La Pacana Caldera (Chilli) area. This study concluded that geologic remote sensing in geothermal systems is not mature and there is a need to integrate it in a geothermal framework. Classification of ASTER imageries for various hydrothermal minerals such as illite, alunite, gypsum, silica content and lake precipitates was carried out during the study.

A study by Munyiri (2016) comprehensively used high-resolution DEM images in the analysis of structures within the Olkaria geothermal complex. The study integrated structural geology, soil gas sampling, and remote sensing to delineate geothermal features within the study area. From his study, it was established remote sensing image analysis can be used to detect hydrothermal alteration zones and map geological evidence. The notable study gap was insufficient data for classification of the Olkaria caldera. He, however, recommended GPS deformation measurements and InSAR studies to assist in the observation of surface deformation caused by magma chamber pressure changes and magma evolution processes.

2.4 Geothermal Factors

The geothermal evidence features that indicate the occurrence of geothermal resources in area are discussed as follow:

2.4.1 Geological Factors

a. Faults, fractures and open fissures

Faults, fractures and open fissures are important surface manifestation features in geothermal systems. The faults may facilitate geothermal fluid flow by providing channels of high permeability or might create barriers to flow by offsetting areas of high permeability (Munyiri, 2016). Faults are prominent structures in the study area and controls subsurface geothermal activities as shown in Plate (2.1).

Plate 2.1: Faults in the study area (Varet, 2017)

These features appear in a linear pattern, resembling drainage features. This makes them suitable for detection using Satellite remote sensing.

b. Craters and caldera (Eruption centers)

Craters are depressions, commonly deep and precipitous, that mark the eruptive vents of volcanoes. They are indicators of underground heat sources. Most of the craters and calderas in the Eburru geothermal complex coexist alongside eruption of silicic rocks like trachyte, rhyolite, and basalts (KENGEN, 2018) as shown in Plate (2.2).

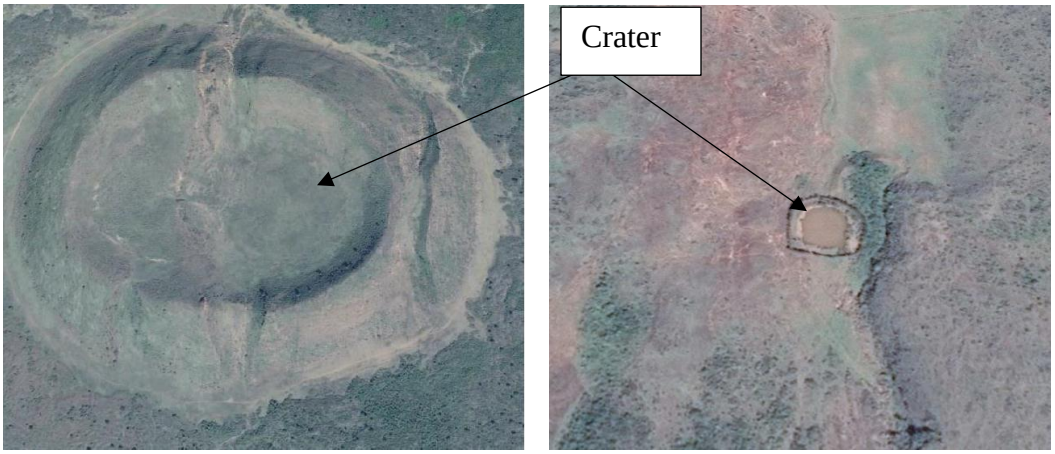

Plate 2.2: Craters in the study area (Varet, 2017)

c. Geothermal index mineral indicators

The common minerals of interest in geothermal fields include alunite, kaolinite, opal, calcite, chlorite, muscovite, gypsum and tincalconite (Littlefield & Calvin, 2014). They have spectral absorption features in the visible to thermal infrared wavelength regions that is related to electronic and molecular vibrations (Haselwimmer & Prakash, 2013). Plate 2.3 shows calcite deposition in the area of study.

Plate 2.3: Calcite deposits observed in the study area (Varet, 2017)

2.4.2 Geochemical Factors

a. Fumarole activity

Fumaroles are vents in the Earth's surface from which steam and volcanic gases are emitted. Fumaroles offer an important window into the processes at work beneath the surface of some volcano (Braddock et al., 2017). Fumarole activities usually follow the structural configuration of faults and fractures in areas of recent volcanism. The manifestations have are used as indicators of the existence of geothermal systems associated with shallow magma chambers (Omenda et al., 1993). The zones are also characterized by the presence of secondary minerals such as kaolinite, montmorillonite clays, silica residue, alunite, alunogen, alumina, and occasional native sulphur. The fumaroles also have elevated temperatures which act as a source of geothermal anomaly suitable for monitoring using Remote sensing techniques. They depict changes linked to hydrological processes such as precipitation and groundwater flow. The hydrothermal system is heated by a deeper magmatic system. The study area is characterized by abundant fumaroles spread as shown in Plate 2.4.

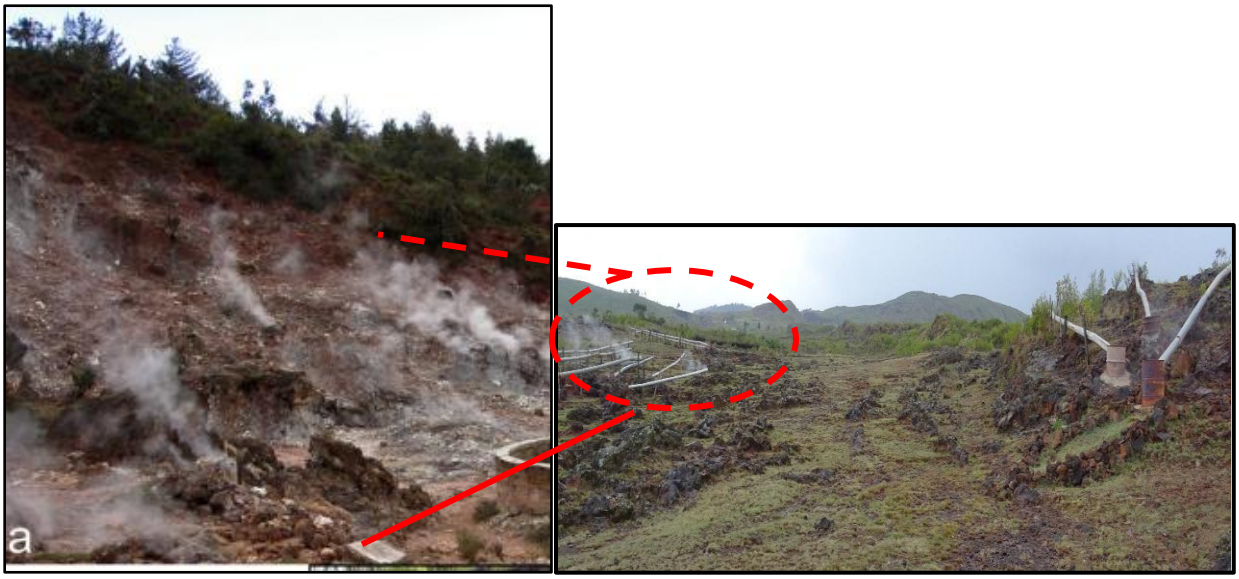

Plate 2.4: Fumarolic activities in the study area (Varet, 2017)

b. Hydrothermal alteration zones

Hydrothermal alteration is a general term embracing the mineralogical, textural, and chemical response of rocks to a changing thermal and chemical environment in the presence of hot water, steam, or gas (Shako & Wamalwa, 2014). Hydrothermal alteration is caused by the processes acting within volcanic systems such as fluid-rock interaction, boiling and mixing are considered

the primary cause of various surface waters and steam vents as well as the observed secondary mineralogy (Bjorke, 2010). Hydrothermally altered zones are in the study area are found along faults as shown in Plate 2.5.

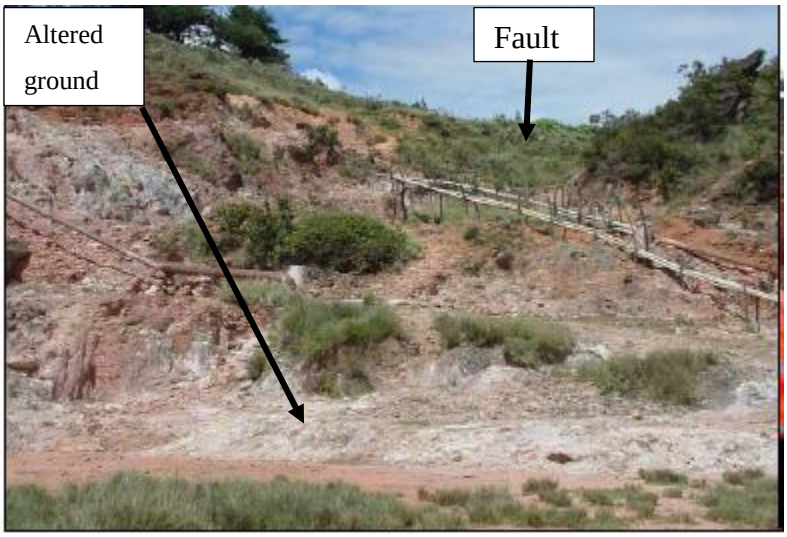

Plate 2.5: Altered Grounds at Eburru area (KENGEN, 2018)

By mapping alteration zones at the surface, it is possible to locate the zones with highest temperatures, pressures, or permeability, all of which are important in geothermal exploration.

2.4.3 Thermal Factors

a. Heat loss measurements

The heat is known as the natural heat loss of the system. By measuring ground temperatures distribution, it is possible to map prospect areas within geothermal systems. Temperatures were taken at shallow holes (50cm-1m) on the land surface at proposed zones within areas of interest and interpolated to establish their spatial distribution.

b. Satellite Land surface Temperature measurements

The earth's surface is composed of selectively radiating bodies such as rocks, water, vegetation that emit a certain proportion of the energy emitted from a black body at some temperature (Jensen, 2013). Emissivity (ε) is the ratio between the actual radiance emitted by a real-world selective radiating body (M_r) and the black body at the same thermodynamics (kinetic) temperature (M_b) (Jacob et al., 2004) as shown in Equation 2.1:

$$\varepsilon = \frac{\mathbf{M}r}{\mathbf{M}b} \ldots\ldots\ldots\ldots\ldots\ldots \textbf{(2. 1)}$$

Surface temperature measurements are performed with a temperature probe and measure the kinetic temperature of the body being measured (Ólafsson, 2018). Kinematic is the internal energy of a concerned object. The objects then radiate the energy as a function of their radiant temperature. Emissivity of objects according to Schmugge et al. (2002), is influenced by factors such as color, chemical composition, surface roughness, moisture content, compaction, field of view, wavelength and field of view. Thermal InfraRed (TIR) remote sensing provides the unique possibility to retrieve surface temperature and broadband emissivity in a spatially distributed manner (Jacob et al., 2004). By knowing earth's surface object emissivity, it is possible to correctly estimate emitted radiance and determine surface land temperature from radiance data. Emissivity is a key factor in LST retrieval. Thermal infrared remote sensing has become an efficient way to estimate land surface temperature (LST) and conduct the exploration of geothermal resources.

Land surface temperature was calculated on a Landsat 8 satellite images acquired over the Eburru area in July 2017. The TIR bands 10 and 11 were used to estimate brightness temperature while bands 4 and 5 were used to generate NDVI. Landsat 8 is useful because it provides metadata of the bands such as thermal constant, rescaling factor value etc., which can be used for retrieval of LST. Land surface temperatures (LST) were estimated from Landsat 8 images acquired on June and September 2017. The thermal bands (band 10 and band 11) of the Landsat images were analysed to identify the LST distribution pattern of Eburru area procedurally as discussed as below:

(1). Top of Atmosphere (TOA) Radiance

The Thermal Infrared digital numbers were converted to TOA spectral radiance using the radiance rescaling factor extracted from the metadata file (Equation 2.2).

$$\boldsymbol{L_x = M_l Q_{CAL} + A_l} \text{ ... ...} \textbf{(2. 2)}$$

Where: L_x = TOA spectral radiance (Watts/m2*s rad*μm)

M_l = Band specific multiplicative rescaling factor from metadata (RADIANCE_MULT BAND X, where x is the band Number)

Q_{CAL}= Quantized and calibrated standard product scale values (DN)

A_l= Band specific additive band rescaling factor from metadata (RADIANCE_MULT BAND X, where x is the band Number).

Conversion of Radiance to (TOA) Brightness Temperature

Conversion of the at-sensor radiance to at-sensor brightness temperature assumes that the Earth's surface is a black body with an emissivity equaling to 1 that includes the atmospheric effects

(Chander et al., 2009). This temperature doesn't reflect the surface temperature. Spectral radiance data can be converted to top of atmosphere brightness temperature using the thermal constant Values in Landsat 8 Meta data file (Chander et al., 2009) as represented by equation (2.3).

$$\boldsymbol{BT} = \frac{\boldsymbol{K_2}}{\boldsymbol{In}\left(\mathbf{1}+\frac{\boldsymbol{K_1}}{l_\lambda}\right)} - \mathbf{273.15} \ldots\ldots\ldots\ldots \textbf{(2. 3)}$$

Where: BT =Top of Atmosphere satellite brightness temperature (^{o} C)

l_λ = TOA spectral radiance (Watts/m2*srad*um)

K_1=Band specific thermal conversion constant from the metadata (K_1_constant_Band x, where x is band number 10 or 11)

K_2=Band specific thermal conversion constant from the metadata (K_2_constant_Band x, where x is band number 10 or 11)

Emissivity calculation using the NDVI threshold formula

The Normalized Differential Vegetation Index (NDVI) was calculated using Near Infra-red (Band 5) and Red (Band 4) bands as represented by Equation (2.4).

$$\textbf{NDVI} = \frac{\textbf{Near infrared (band 5)} - \textbf{Red(band 4)}}{\textbf{Near infrared+Red}} \ldots\ldots\ldots\ldots\ldots \textbf{(2. 4)}$$

Where: RED= DN values from the RED band NIR= DN values from Near-Infrared band

Land surface emissivity (LSE) which is the average emissivity of an element of the surface of the Earth calculated from NDVI values (Equation 2.5). For the Landsat 8 OLI-TIRS images, the daytime OLI images were used to estimate the spectral emissivity of each land cover of the study area.

$$\boldsymbol{\rho v} = \left(\frac{(\boldsymbol{NDVI - NDVI_{min}})}{(\boldsymbol{NDVI_{max} + NDVI_{min}})}\right)^{\mathbf{2}} \ldots\ldots\ldots\ldots\ldots \textbf{(2. 5)}$$

Where: PV = Proportion of Vegetation

NDVI = DN values from NDVI Image

NDVI min = Minimum DN values from NDVI Image

NDVI max = Maximum DN values from NDVI Image

Emissivity is calculated as follow.

$$\textbf{Emissivity } (\varepsilon) = \mathbf{0.004} * \boldsymbol{\rho v} + \mathbf{0.986} \ldots\ldots\ldots\ldots \textbf{(2. 6)}$$

Where: ε = Land Surface Emissivity ρv = Proportion of Vegetation

Land Surface Temperature (LST)

The Land Surface Temperature (LST) is the radiative temperature which calculated using Top of atmosphere brightness temperature, Wavelength of emitted radiance, Land Surface Emissivity represented by Equation 2.7.

$$Land\ Surface\ Temp\ = \frac{BT}{1+W\left(\frac{BT}{P}\right)*In(\varepsilon)} \ldots\ldots\ldots\ldots\ldots\ldots\ldots \textbf{\textit{(2. 7)}}$$

Where: BT=Satellite temperature,

W=Wavelength of the emitted radiance (11.5 μm),

$P = h * c/s(1.438 * 10^{-2} m\ K$

h is Planks constant ($6.626*10^{-34}\ JS$)

s is the Boltzmann Constant ($1.38*10^{-23}$ J/K)

c=velocity of light ($2.98 *10^{8}\ m/s$)

ε is the land surface emissivity

2.5 Geothermal well site suitability selection process

The key to successful drilling of any type of geothermal well is correct siting and design for the well based on clear definition and understanding of the drilling target aimed for (Gudni & Hjalti, 2012). Geothermal well site suitability selection involves multi-criterion decision making done by integrating surface exploration datasets ranging from geological (faults/fractures), geochemical data (altered grounds, fumaroles, hot grounds) and thermal anomalies (heat loss surveys, land surface emissivity) in a GIS platform. The output is a suitability map envisaging where the geothermal well sites can be best located within the social-ecological-technical conflict landscape. Siting of geothermal wells is a spatially explicit process based on multiple criteria (Fargione, Slaats, & Olimb, 2012); (Araneo & Vergine, 2015). GIS-based tools for multi-criteria analysis enables planners and decision makers to prioritize among alternative strategies, thereby avoiding potential conflicts and enabling a more inclusive and transparent planning process (Simao, Densham, & Haklay, 2009); (Ciaccia, Doni, & Fontini, 2010). The first step of GIS multi-criteria analysis is to identify the relevant criteria pertaining to decision-making process. For this study, the applicable criteria include proximity to geological structures, distance to surface expressions and thermally suitable areas or hotspots. The multi-criteria evaluation process using GIS is procedurally discussed as follow:

2.5.1 Problem definition

The process of geothermal well site selection begins with the recognition of an existing or projected need. At this stage, the project goal is defined. This recognition triggers a series of actions that starts with the screening of geographic areas of specific interest (Al-Amri & Eldrandaly, 2014).

2.5.2 Definition of Constraints

Constraints are areas that limit or make expansion and investment impractical according to Best Management Practices and development guidelines. Constraints analysis is based on the Boolean criteria, which limit the alternatives under consideration to specific regions (Sarpong & Baffoe, 2016). They are expressed in the form of a Boolean (logical) map where areas excluded from the consideration (i.e. unsuitable areas) are coded with the value 0 and those open for consideration (i.e. suitable areas) are coded 1 (Sarpong & Baffoe, 2016; Chaudhry, 2008).

The following are the set constraints for this study:

i. Siting is restricted to regions 1000m away from residential areas (Yousefi et al., 2007). This is to reduce pollution arising from drilling of geothermal wells or any modification to the landscape.
ii. Geothermal wells cannot be sited in protected areas such as forest and game reserves, tourist sites, (Noorollahi, 2005).
iii. Siting in lakes or any water body is restricted (Chaudhry, 2008) to avoid pollution resulting from injection of brine into the water source. Sarpong & Baffoe (2016) proposed a 250m buffer of streams and water bodies.

2.5.3 Definition of criteria

Sites that satisfy the screening criteria are subjected to more detailed evaluation and are compared as possible alternative sites for the proposed facility. Usually, the screening criteria would include economics, social, and environmental measures/factors (also known as constraints). Normalization of the proxy criteria. The involved criteria are often multiple and incommensurable because they have different objectives measured along quantitative, qualitative, discrete or continuous measurement scales. To make the different criteria proxies comparable along a common measurement scale, they must be normalized using a scale function (Hannssen et al., 2018). The involved criteria should be as far as possible also be made comparable at a common spatial scale and resolution (Hannssen et al., 2018).

2.5.4 Standardization of Criteria

The classification and value of all the criteria maps are converted into a common scale in which there is a uniform value function as appreciated by the decision maker (Mwaura, 2018). The classification for each factor map involved creating five value ranges, a method adopted from Trumpy et al. (2015) in their classification of similar geothermal evidence layers. Each layer of data is created as multi-class evidence map with each class being assigned a score indicating the level of suitability (Mwaura, 2018). Standardization for most of the factor maps was done using a linear function, which converted the original factor scores (each expressed in its own unit of measurement) into dimensionless scores in the range 1 (Least suitable) to 3 (Most Suitable) in increasing suitability.

2.5.5 Criteria weighting

Weighing was done after standardization of criteria values. Different methods were used to assign weights to criteria. The main methods of assigning weights to criteria as follow:

1.) Ranking method: Consideration ranked according to the considerations of the decision maker's preferences.

2.) Rating method: Requires the estimation of weights on the basis of the predefined scale.

3.) Pairwise comparison method which involves the creation of a ratio matrix.

4.) Trade-off analysis method which makes use of the direct trade-off assessment between pairs of alternatives.

2.5.6 Aggregation of the geothermal well selection factors

The various criteria (geological, geochemical and thermal) factors were aggregated to obtain a combined factor map. The simple overlay, Boolean overlay and weighted index ovelay techniques were used for spatial multi-criteria combination of the geoscientific factors. This was done based on assigned percentage of influence according to its importance.

CHAPTER THREE

3 MATERIALS AND METHODS

3.1 Study area

The study area is located in Nakuru County, about 150 km NW of Nairobi, Kenya. It is bounded by longitudes 36 ° 07’ 30.0” and 36 ° 18’ 00.0” E; and latitudes 0 ° 34’ 30.0” and 00 ° 40’ 00.0” S; covering an area of approximately 360 km ^{2} as shown in Figure (3.1). It bounds Lake Elementaita to the North.

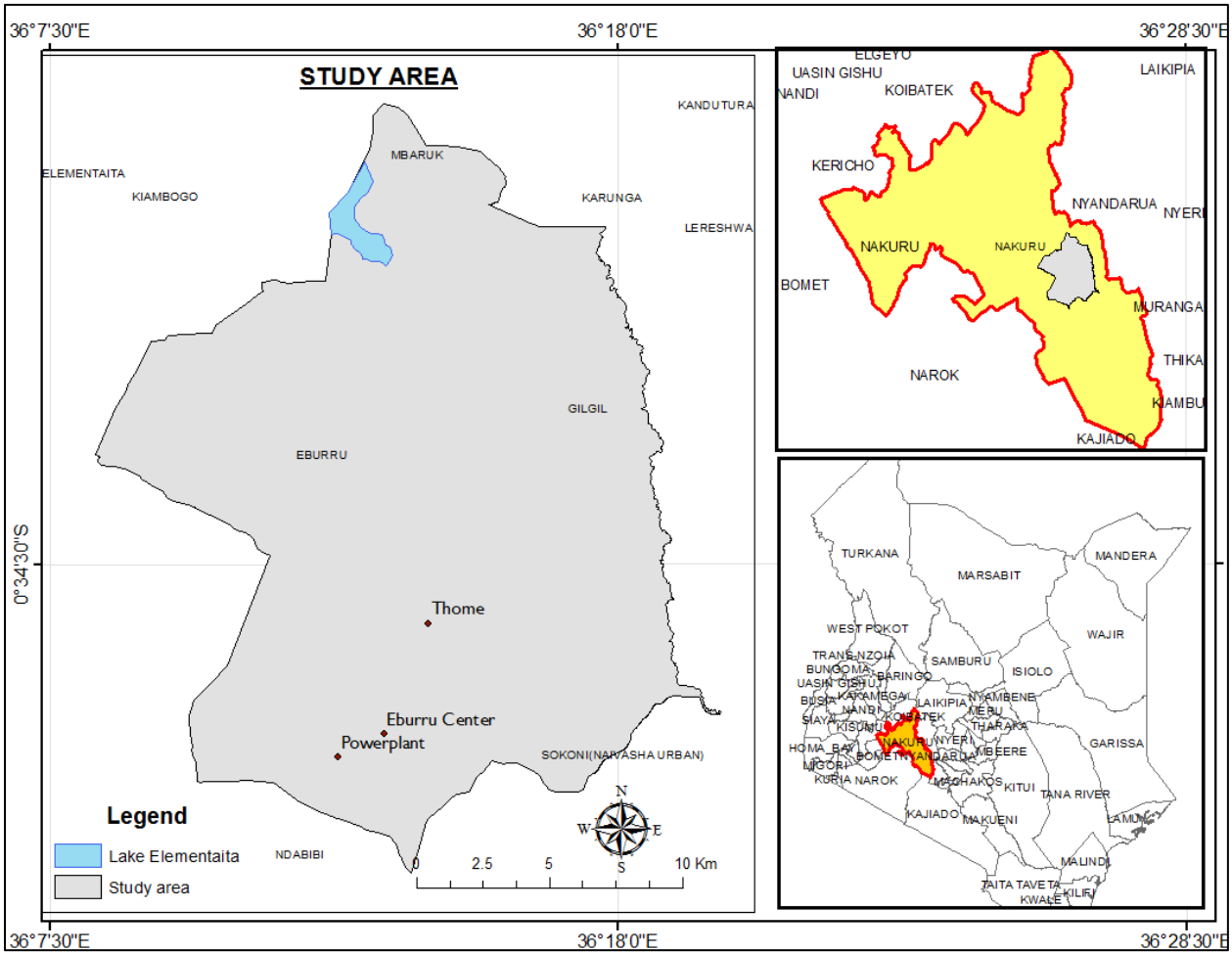

Figure 3.1: Location of the study area

3.2 Data types and sources

The data sources for this study are summarized in Table 3.1

Table 3.1: Data sources for the study

Data Type	Source	Format	Spatial Resolution/scale
Landsat 8	https://earthexplorer.usgs.gov/	Raster (Geotiff)	30m (multispectral), 15m (panchromatic)
Landsat 7 ETM	https://earthexplorer.usgs.gov/	Raster (Geotiff)	30 m
DEM/SRTM	www2.jpl.nasa.gov/srtm	Raster (img)	30m
Geological map	Mines and Geology Department	Raster(img)	1:125,000
Topographical map	Survey of Kenya	Raster(img)	1:50,000

3.3 Procedure

3.3.1 Data collection methods

This is the process of data collection of various geothermal evidence datasets for the proposed study. The datasets were collected in the following ways:

- Primary data such as GPS field measurements of various geothermal evidence features.
- Secondary data such as Digital elevation models, geological maps and topographical maps and satellite Remote sensing data

3.3.2 Re-projection and transformation

Re-projection and transformation was done to the relevant dataset to register them into a uniform coordinate system. Geological data and topographical data layers were digitized to delineate boundaries of the various features in the area of study. The raster datasets were converted to vector formats (points, polylines, and polygons) for further processing.

3.3.3 Image pre-processing and enhancement

Various techniques such as panchromatic sharpening (pan sharpening) and band composite were used to digitally enhance the raw Landsat 8 satellite images in order to obtain the best images for further analysis.

3.3.4 Analysis

GIS spatial analyst methods such as Euclidian distance estimation, extraction (clipping, masking), and reclassification based on various weighting criteria of the factors discussed in the literature review.

3.3.5 Information presentation and interpretation

Results of the weighting and reclassification processes were used to develop suitability maps which were then presented in form of enhanced images and metadata tables.

The aforementioned processes are represented in Figure 3.2.

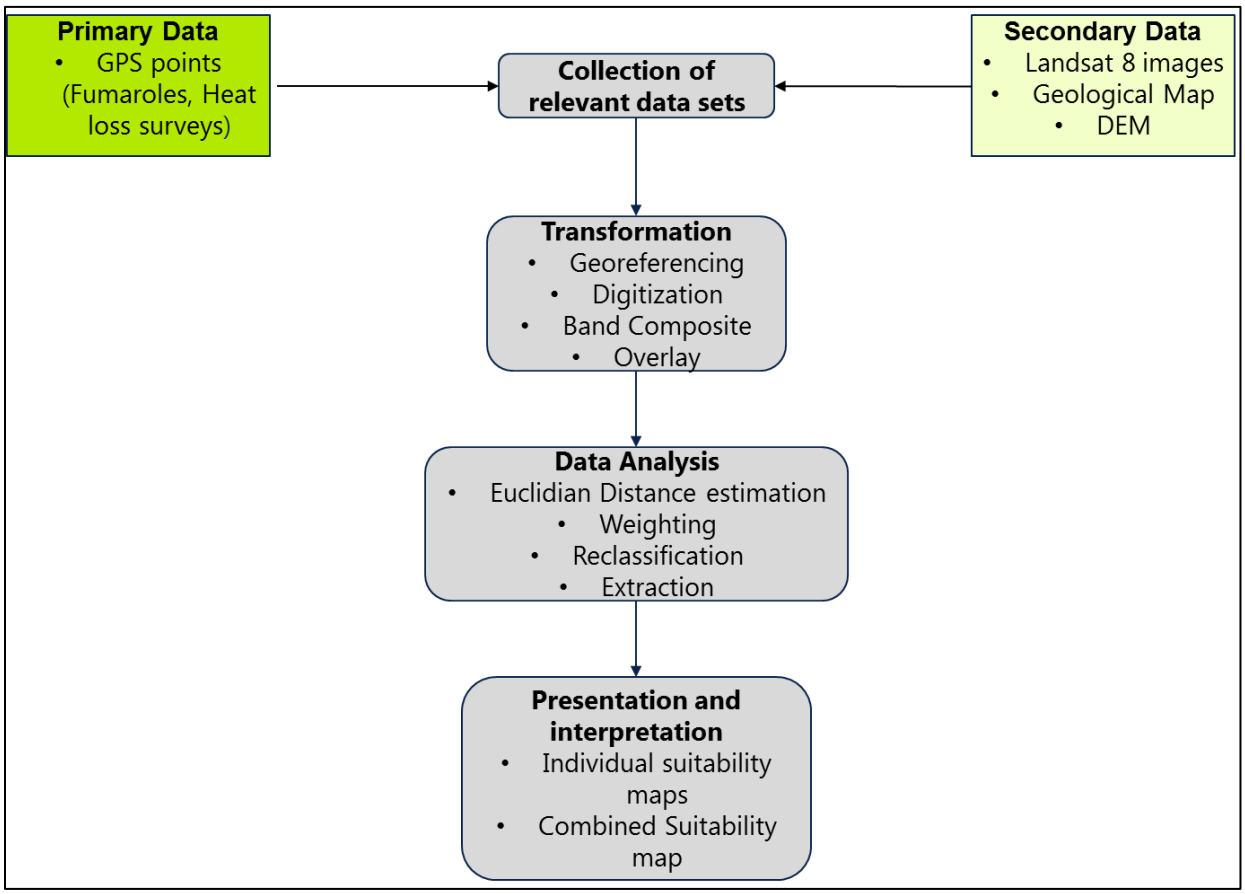

Figure 3.2: Schematic workflow of the data processing

A detailed conceptual framework was developed based on the factors and constraint criteria that were discussed in literature review as shown in Figure (3:3).

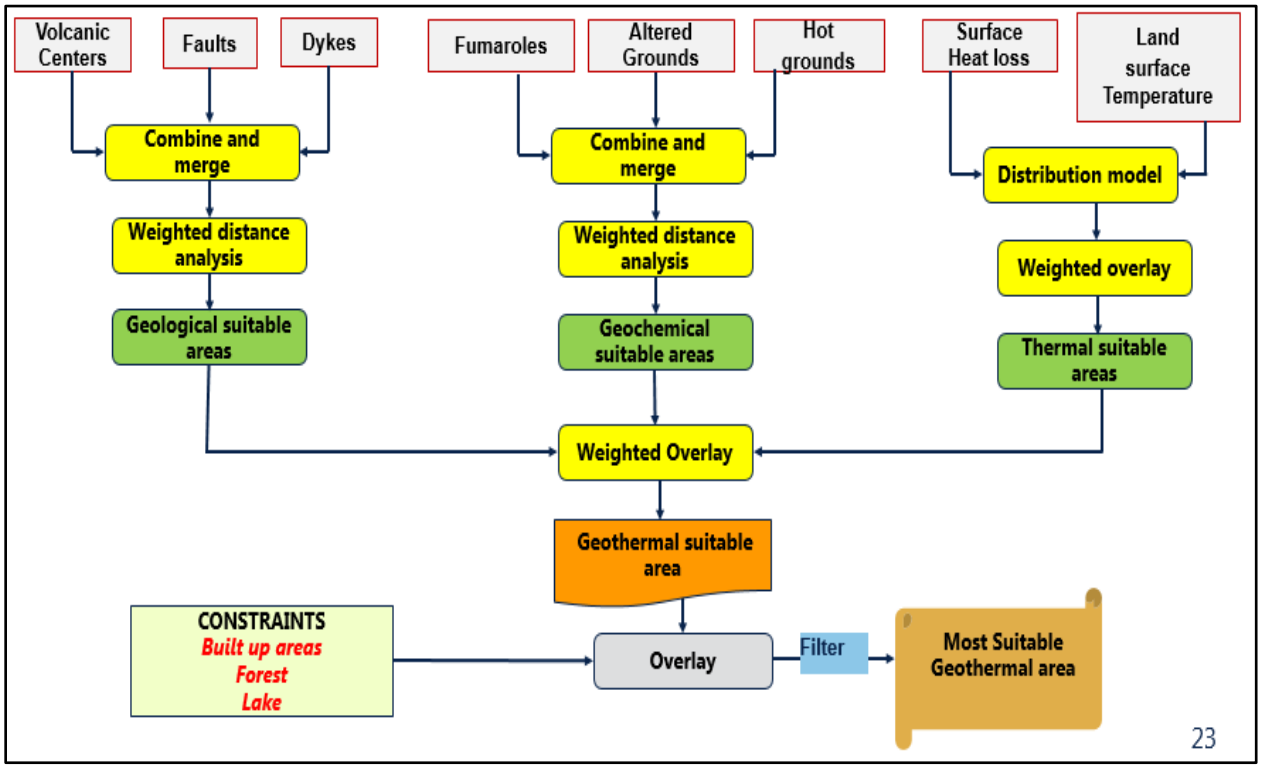

Figure 3.3: Flow diagram showing steps used to identify suitable sites for geothermal wells

3.4 Overview of the study methods

3.4.1 Remote sensing techniques

a. Band composite and Image Pan sharpening

Pan sharpening was done to merge the high-resolution panchromatic band 8 of the Landsat 8 OLI image with a lower resolution multispectral imagery (Bands 2, 3, 4, 5, 6) to create a single high-resolution color image.

The pan sharpened bands of the satellite images were combined in form of color composite images. An RGB 5:4:3 combination was used to create a true color image. In this image, the alteration zones were identified as (brown), vegetated areas as green, rivers and lakes as blue as shown in Figure 3.4. The false color composite image was created by RGB combination 4:3:2. From the image (Figure 3.5), altered areas were discriminated as white to creamy color, vegetation appeared in shades of red, urban areas as blue while the bare surface appeared brown in color.

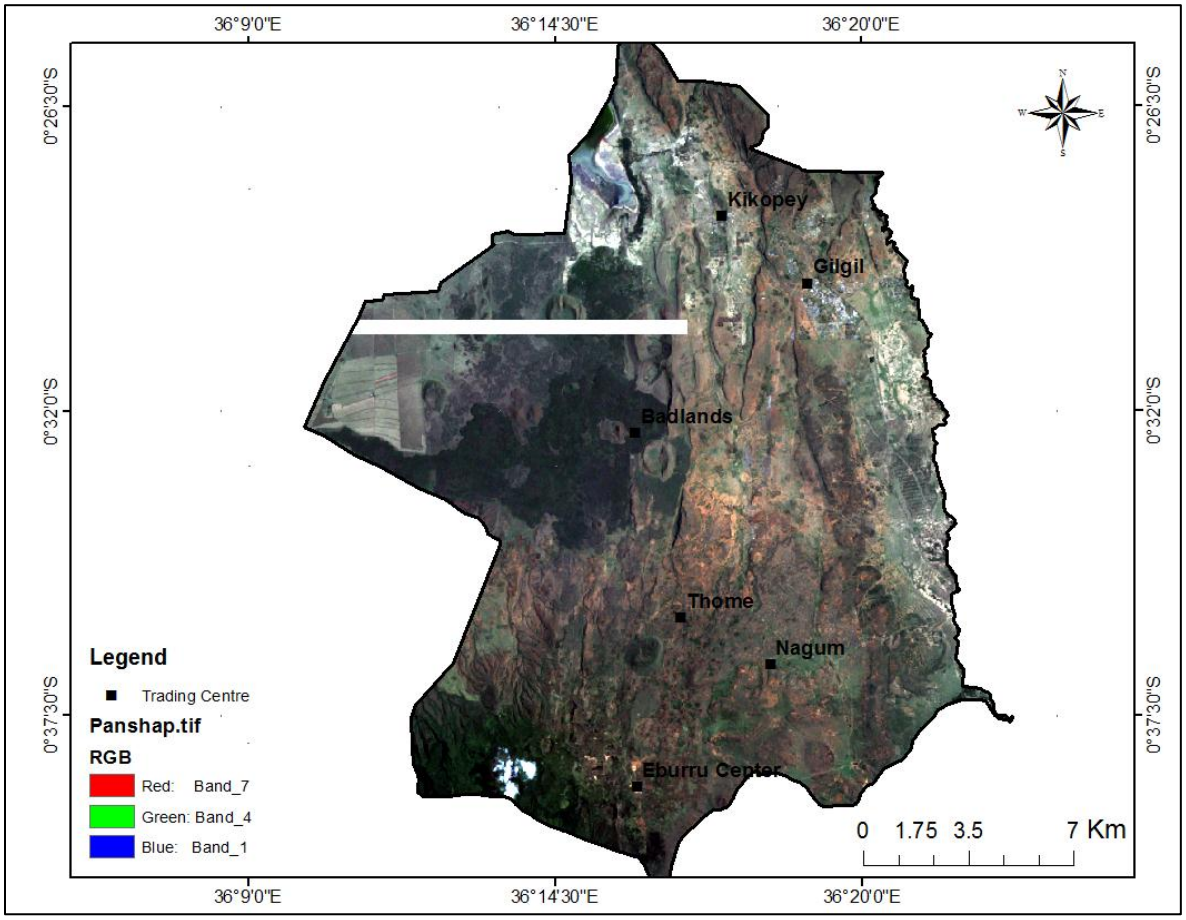

Figure 3.4: True color composite map of Eburru area

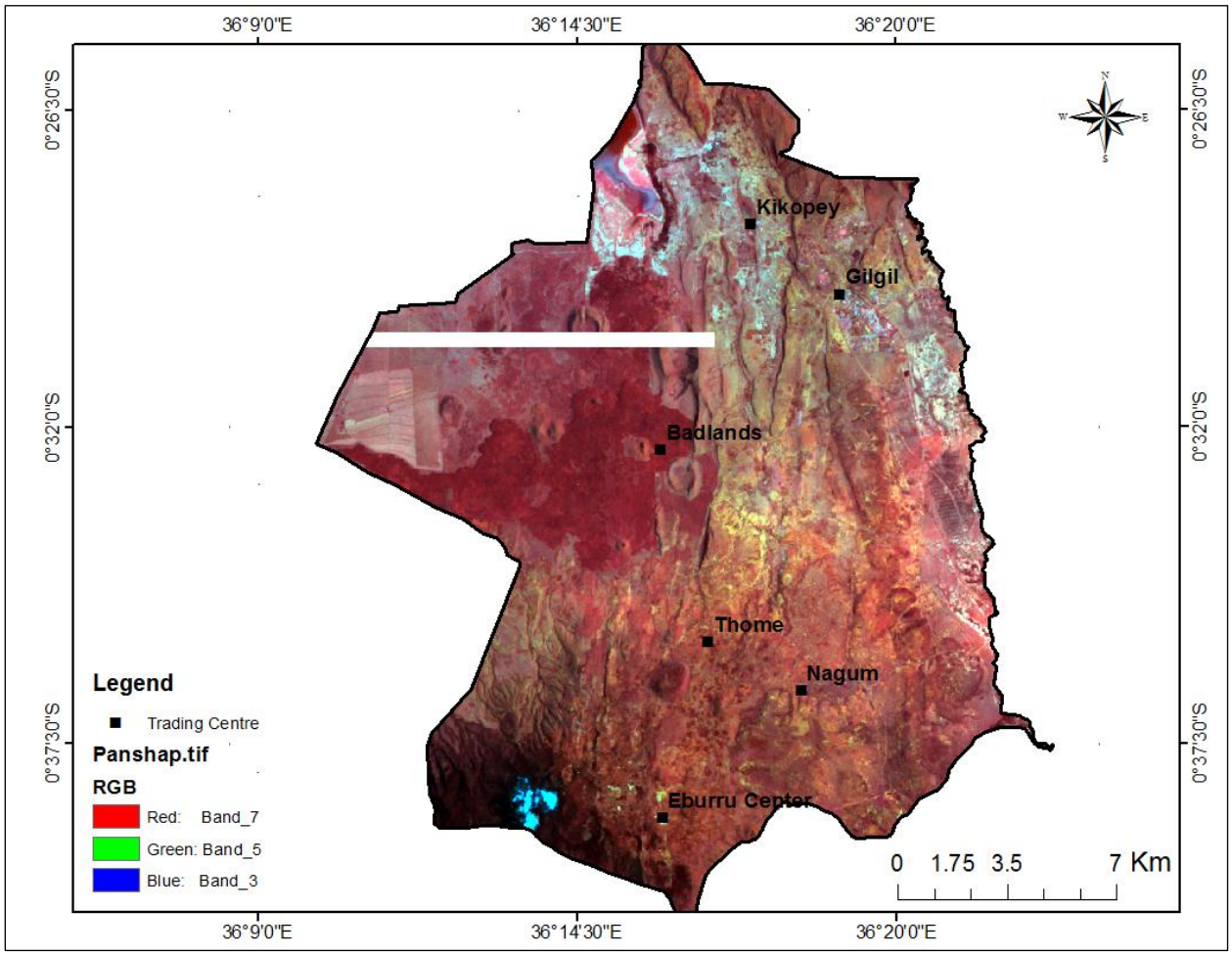

Figure 3.5: False color composite map of Eburru area

3.4.2 GIS techniques

As discussed in the literature review, the following GIS techniques were used for the study:

a. Digitization and conversion of vector to raster

The original data sets collected from the field were digitized in the form of points, poly lines and polygons. Geological features such as eruption centers, dykes and faults were digitized from enhanced Landsat 8 satellite imagery as shown in Figure 3.6.

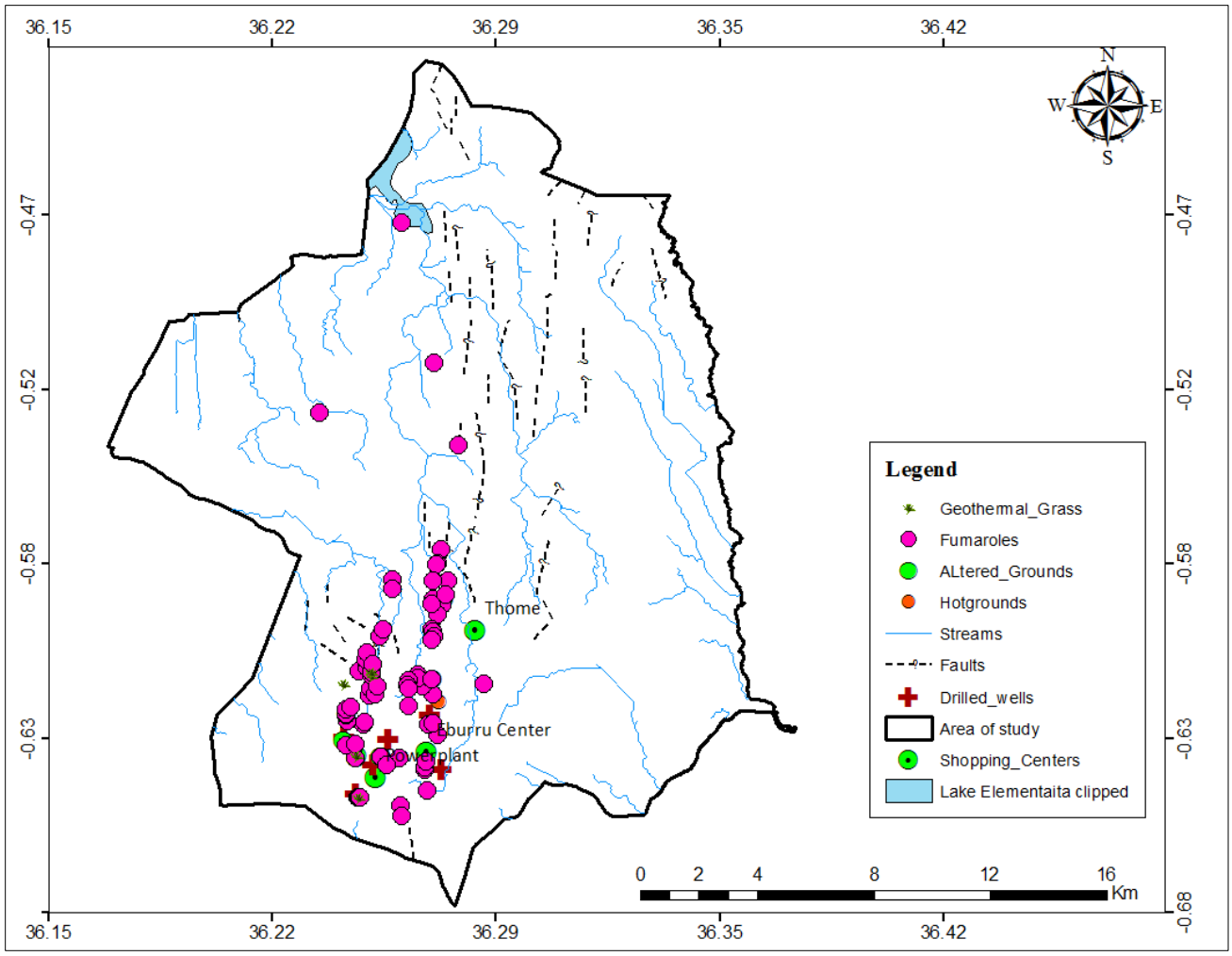

Figure 3.6: Digitized map of study area

b. Euclidian distance analysis

Euclidean distance analysis was done to establish proximity geothermal factors such using the spatial analyst straight line distance function in ArcGIS 10.5. Respective geothermal factor distance maps were created and represented in Figures (3.7, 3.8, 3.9 and 3.10).

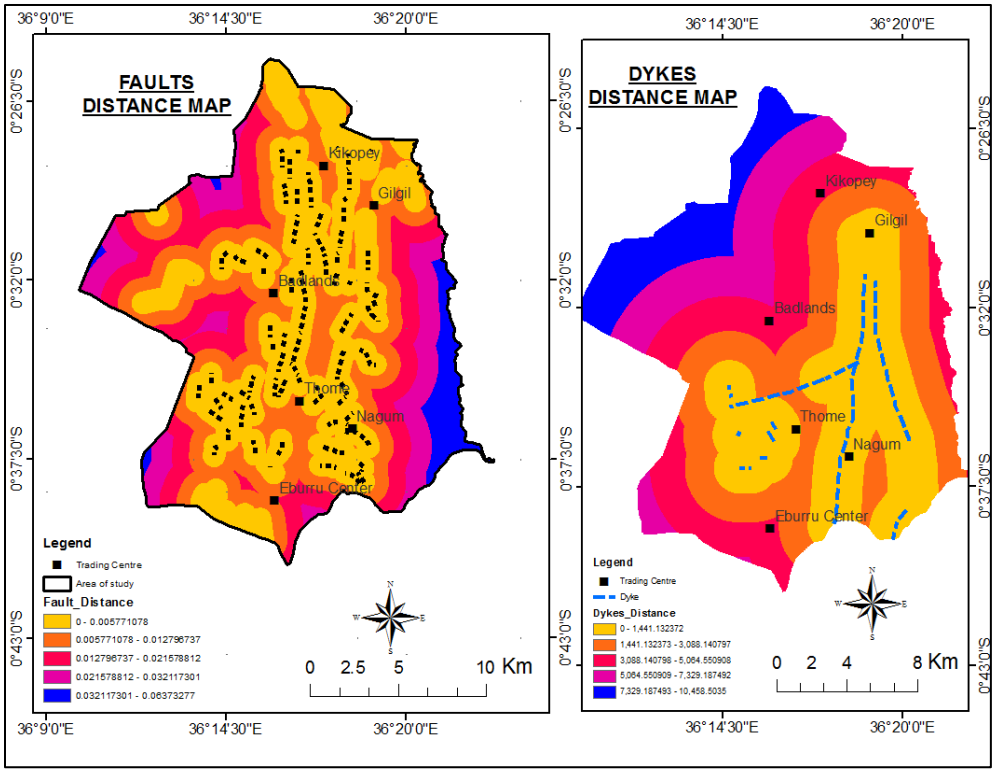

Figure 3.7: Geological distance factor maps (Faults and dykes)

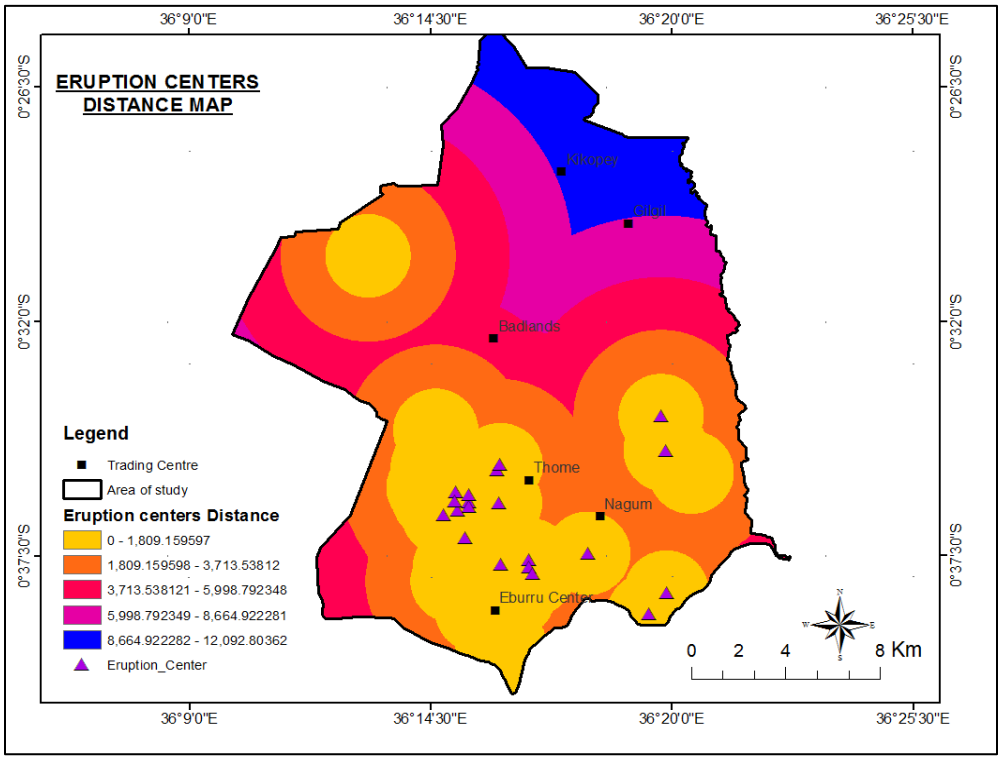

Figure 3.8: Geological factor distance map of the study area (Eruption centers)

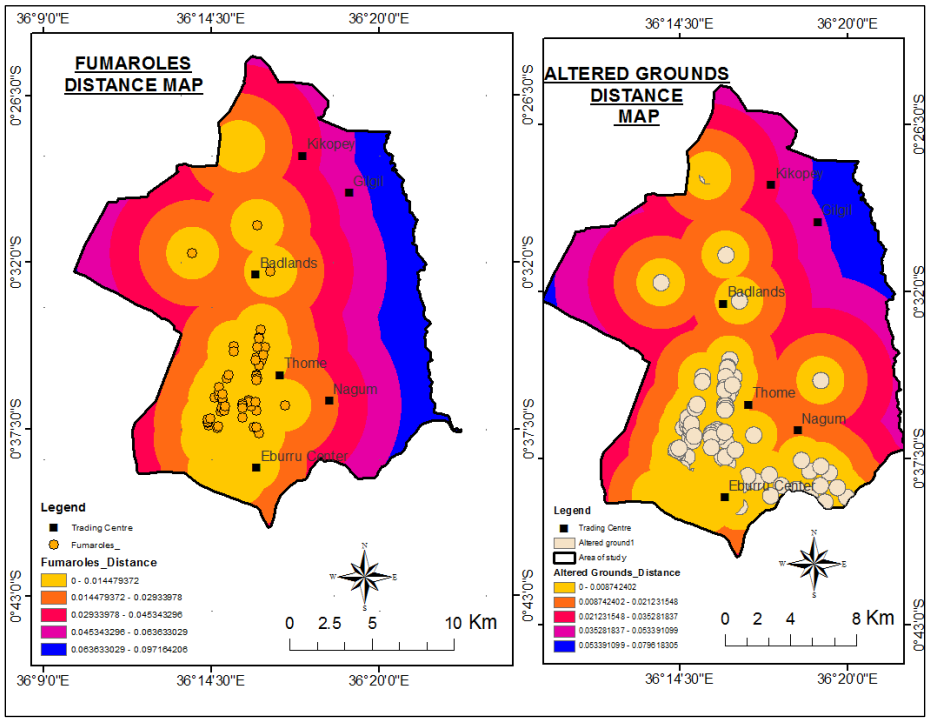

Figure 3.9: Geochemical factor distance map of the study area (fumaroles and altered grounds)

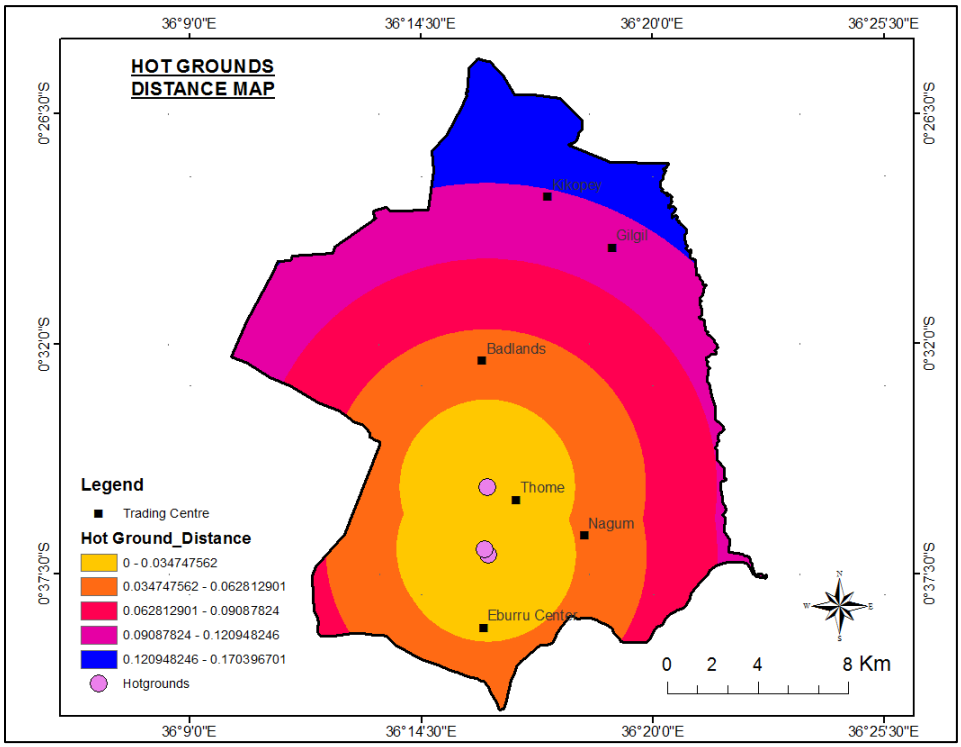

Figure 3.10: Geochemical factor distance Map of study area (Hot grounds)

a. Reclassification of the distance maps

Reclassified maps were created using integer values in a weighted model. It was necessary to assign values of priority to the various criteria factors involved. A value of 4 was assigned to the most suitable range while 1 to the least suitable range for geological factors. The geochemical factors were reclassified into three zones, with a value of 3 assigned to the highest suitability, while a value of 1 was given to the least suitable areas. Reclassified maps were created using the 'Reclassify' function of the GIS spatial analyst tool in ArcGIS 10.5. The reclassified maps are represented in Figure (3.11, 3.12 and 3.13).

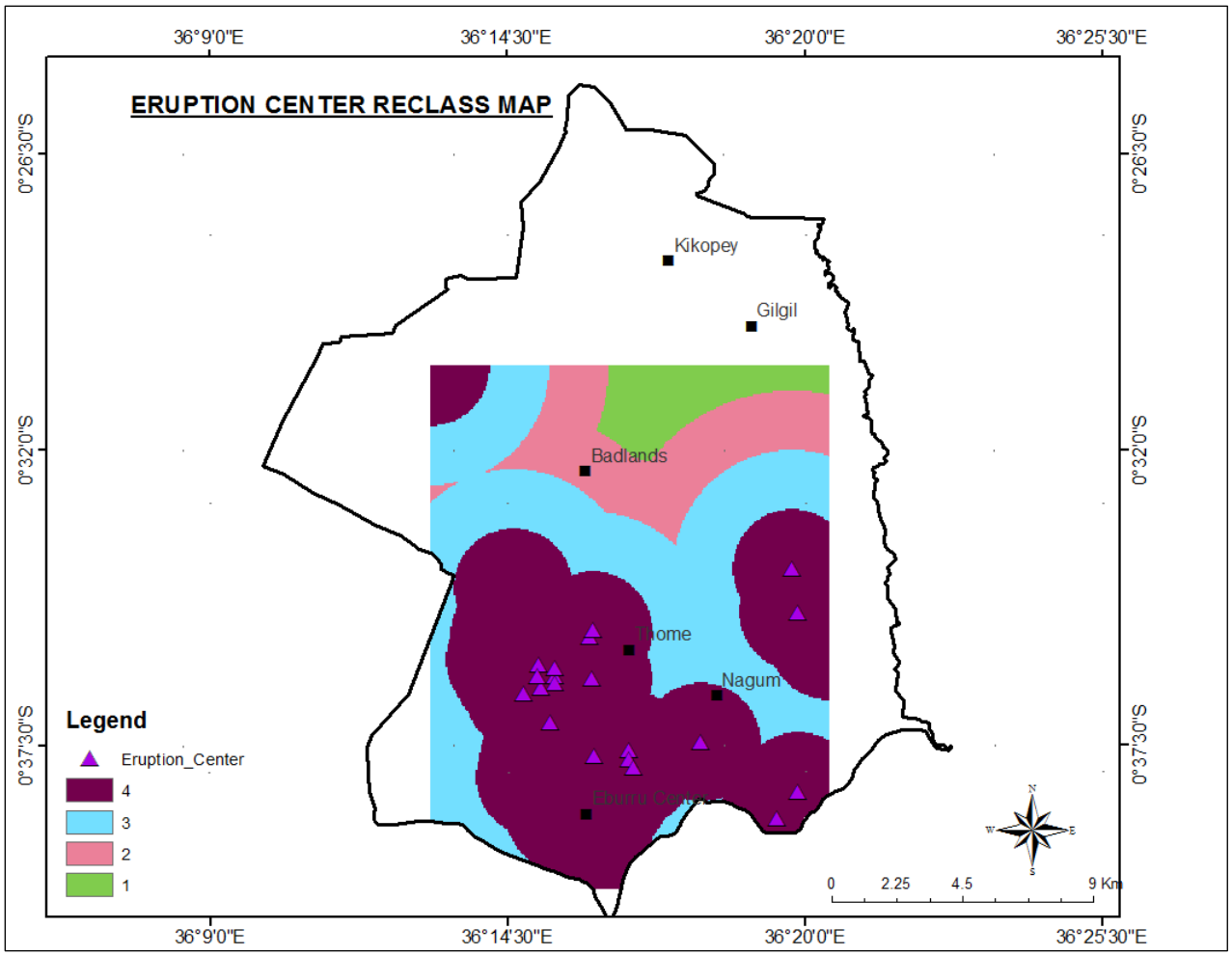

Figure 3.11: Eruption Centers reclassified map of the study area

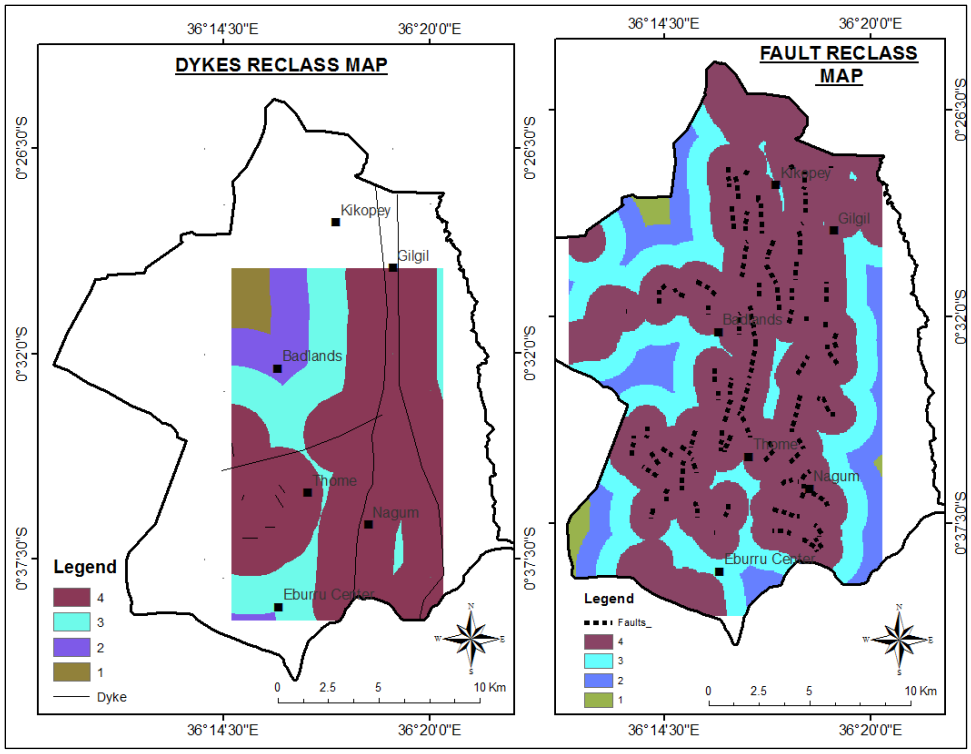

Figure 3.12: Dykes and faults reclassified maps of study area

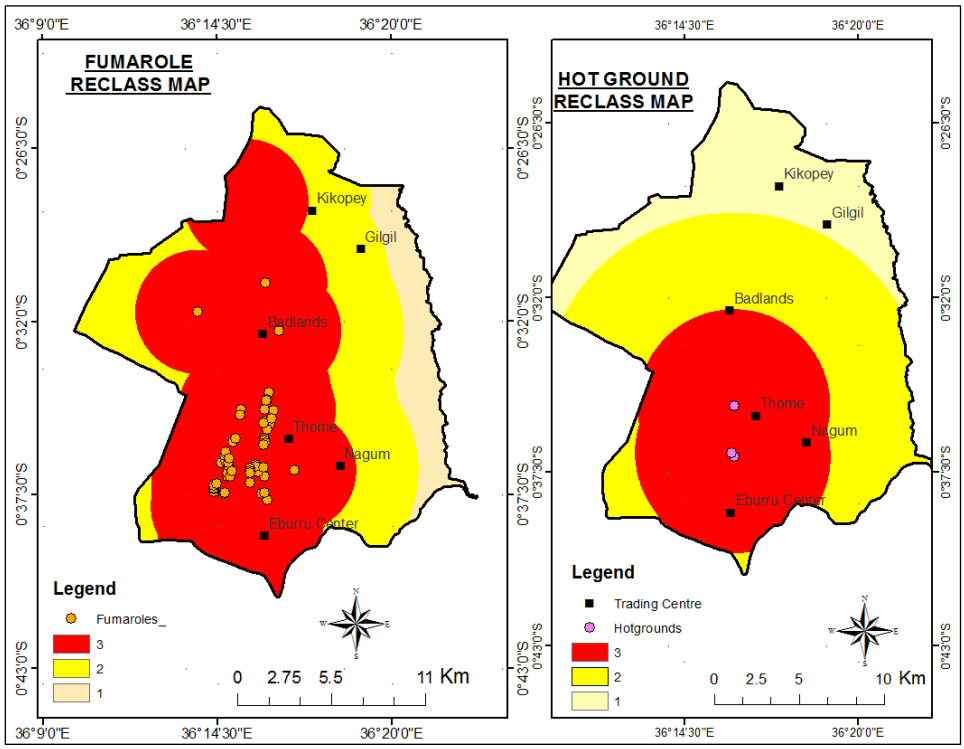

Figure 3.13: Fumaroles and hot grounds reclassified maps of the study area

b. Spatial interpolation and Land surface temperature estimation by NDVI threshold

A temperature distribution model was created by interpolating field heat loss survey values acquired in the area of study using the Inverse Distance Weighted (IDW) method. This was done to establish temperature values unknown zones in the study area.

Land surface temperature was estimated on a Landsat 8 image acquired in June 2017 using the using the NDVI threshold method discussed in chapter two. Two maps were generated as represented in Figures 3.14 and 3.15.

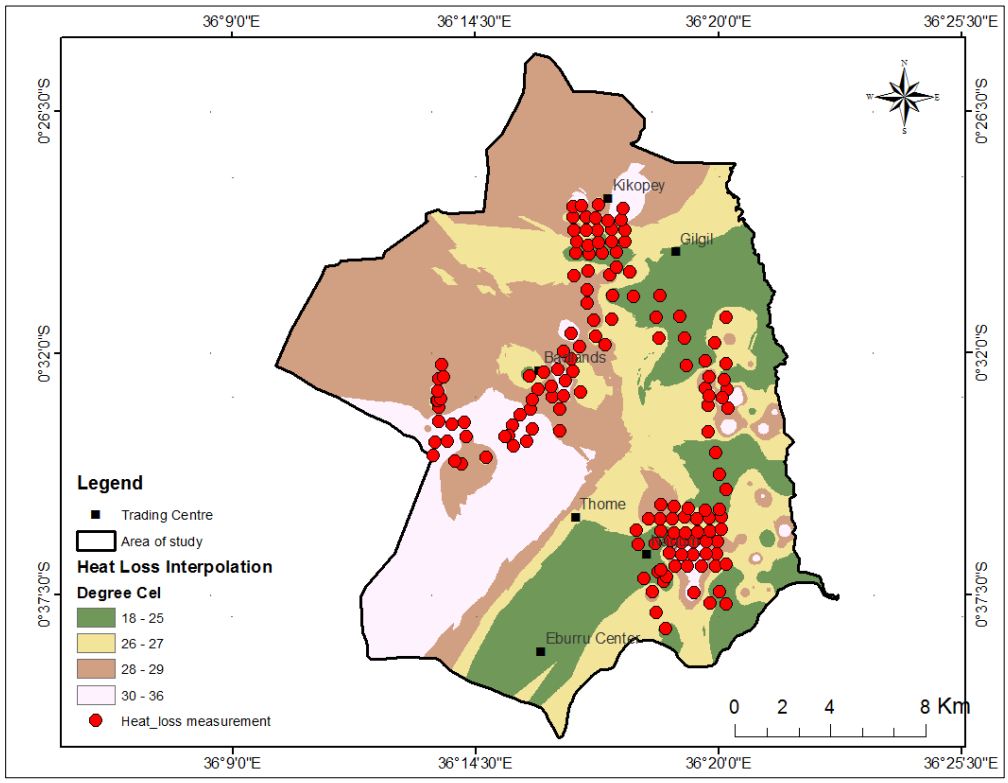

Figure 3.14: Interpolated heat loss survey map of study area

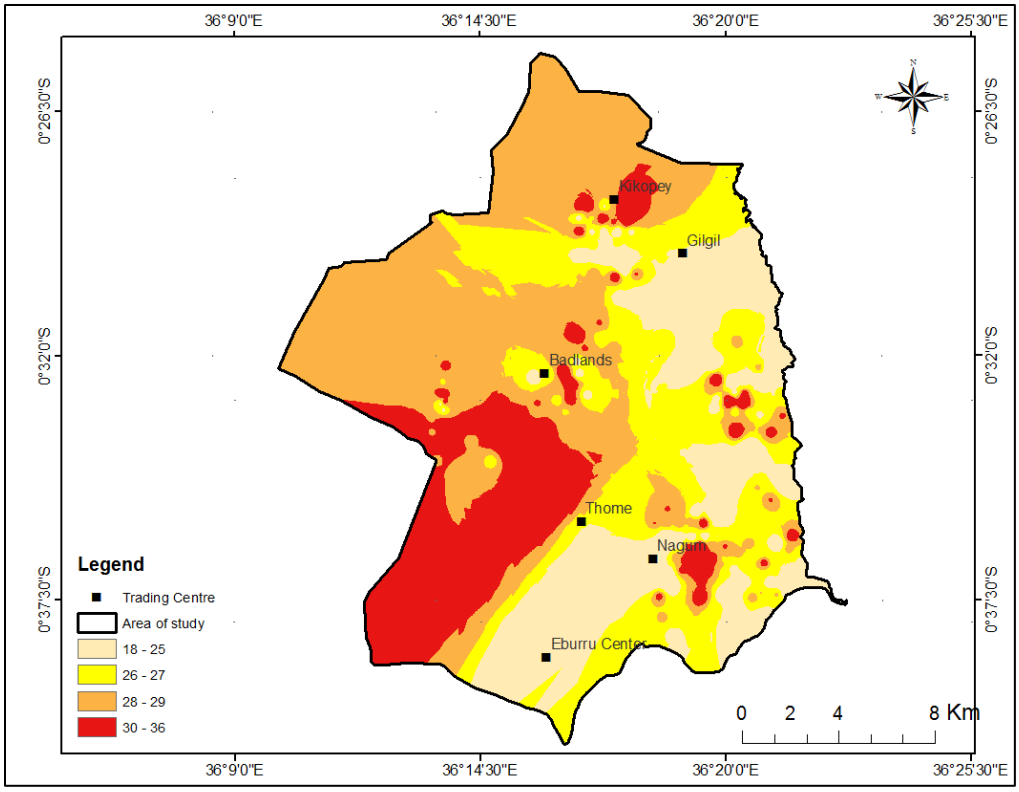

Figure 3.15: Land surface temperature map of study area

c. Weighted Overlay Analysis (WOA)

Weighted overlay analysis was performed on the reclassified maps as follow: (1) Each raster layer was assigned a weight, (2) Values in the rasters were reclassified to a common suitability scale, (3) Raster layers were overlaid, multiplying each raster cell's suitability value by its layer weight and totaling the values to derive a suitability value and (4) the values are written to new cells in an output layer as shown in Figure 3.16.

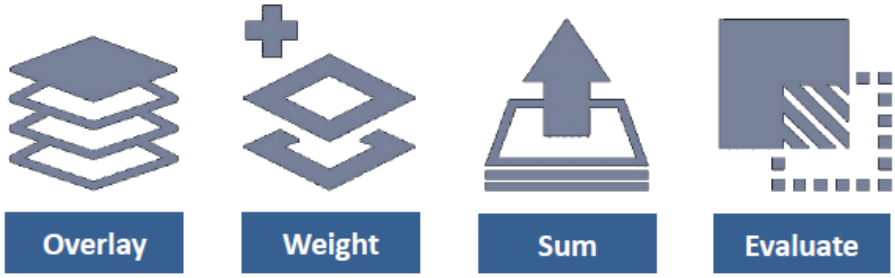

Figure 3.16: Weighted overlay analysis process

3.5 Individual suitability determination Criteria

Individual suitability maps were developed based on the factors discussed in the literature review. The factors include: constraints, geological, geochemical and thermal suitability maps. The factor maps were displayed using three uniform colors as shown in Table 3.2.

Table 3.2: Color codes for suitability ranking

Colors for suitability ranking		
Color	**Description**	**Score**
Red	Most suitable	3
Brown	Moderately suitable	2
Green	Least Suitable	1

The aforesaid factor criteria are discussed as follow:

3.5.1 Constraint Criteria

The environmental constraints were identified and tabulated in Table 3.2.

Table 3.3: Selected constraints for the study area

Geothermal suitability constraints	
Dataset	**Criteria**
Built up areas	1000m buffer
Forested area	250m buffer
Lake/water body	250m buffer

Based on the above criteria, a restriction map was created as represented in Figure 3.17.

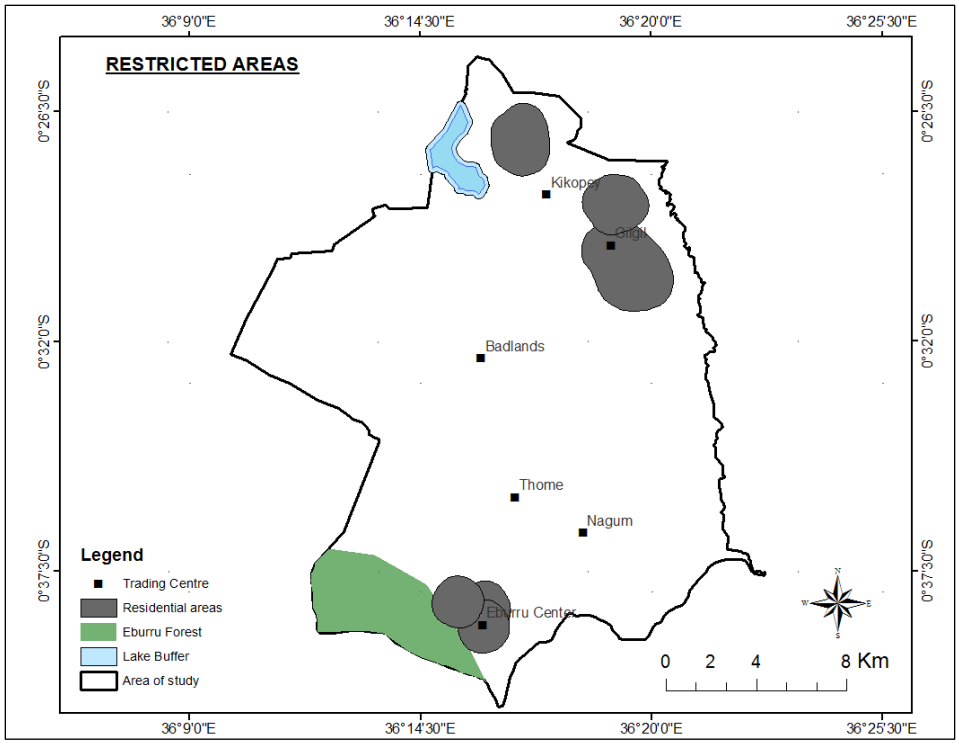

Figure 3.17: Restricted zones of the study area

A binary map was thereafter developed based on the aforementioned constraints as shown in Figure 3.18.

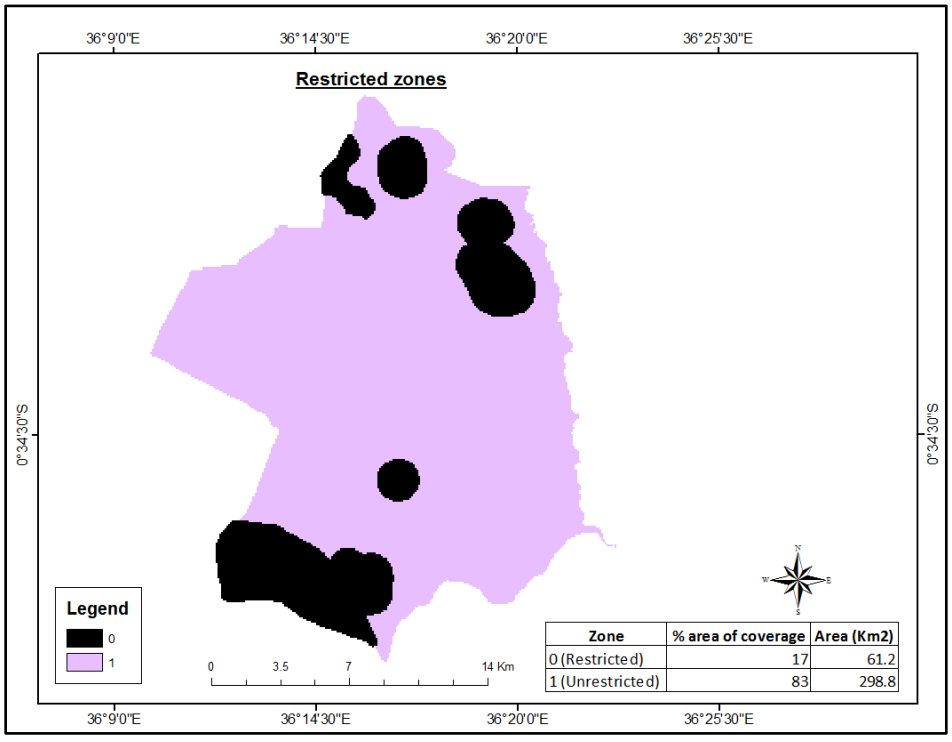

Figure 3.18: The constraint map

From the constraint map, the purple colored areas (coded 1) are considered suitable while the black areas (coded 0) are unsuitable. After developing a restriction model, the zone deemed suitable regions reduced by 17% as shown in Table (3.4).

Table 3.4: Area of the restricted zones

Zone	% area of coverage	Area (Km^2)
0 (Restricted)	17	61.2
1 (Unrestricted)	83	298.8

3.5.2 Geological Suitability

A suitability map was developed based on reclassification and weighting and overlaying of the study's selected geological factors (faults, eruption centers, dykes). They observed geological factors were then classified based on their influence on the existence of geothermal resource as shown in Table (3.5, 3.6 and 3.7).

Table 3.5: Classification of faults and influence on geothermal activity (Yousefi et al., 2007)

Geological: Proximity to Faults [m]		
Distance	**Category**	**Score**
>1600	Least suitable	1
1200-1600	Moderately suitable	2
>1200	Most Suitable	3

Table 3.6: Classification of eruption centers and influence on geothermal activity(Yousefi et al., 2007)

Geological: Proximity to eruption centers [m]		
Distance	**Category**	**Score**
>1600	Least suitable	1
1200-1600	Moderately suitable	2
800-1200	Suitable	3

Table 3.7: Classification of dykes and influence on geothermal activity (Yousefi et al., 2007)

Geological: Proximity to dykes [m]		
Distance	**Category**	**Score**
>1600	Least suitable	1
1200-1600	Moderately suitable	2
>1200	Suitable	3

The above-mentioned factors were overlain and combined using the union tool in ArcGIS 10.5 to identify geologically suitable areas as illustrated in Figure 3.19.

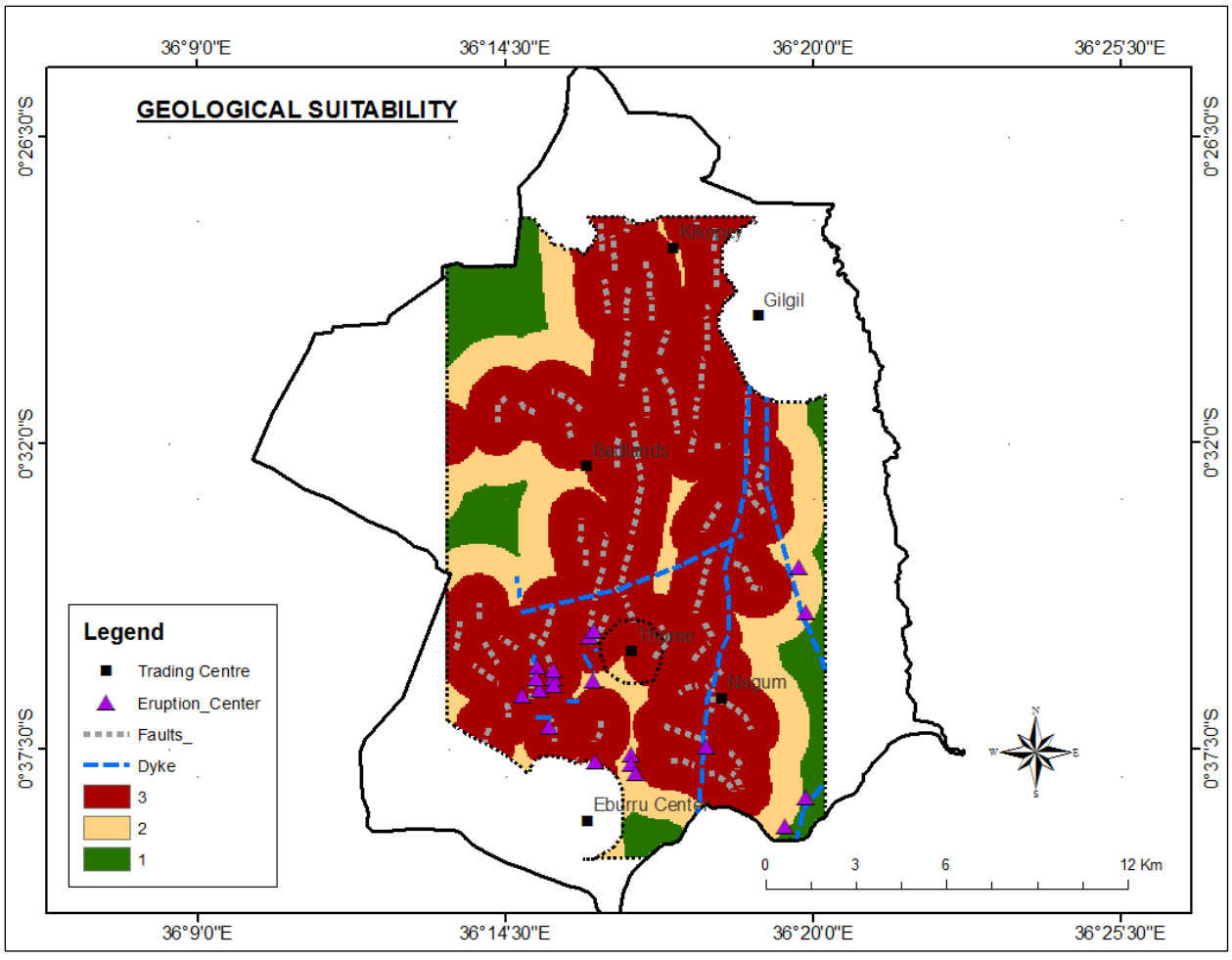

Figure 3.19: Map showing the Geological Suitability of the study area

3.5.3 Geochemical suitability map

The proximity to geochemical features (Fumaroles, altered grounds, hot grounds) was considered in the creation of geochemical suitability maps. The geochemical features were weighted

according to their influence on the existence of geothermal resource in the study are as showb in Table (3.8, 3.9 and 3.10).

Table 3.8: Classification of fumaroles and influence on geothermal activity (Yousefi et al., 2007)

Geochemical: Proximity to fumaroles [m]		
Distance	**Category**	**Score**
Greater than 4000	Least suitable	1
2000-3000	Moderately suitable	2
1000-2000	Most Suitable	3

Table 3.9: Classification of altered grounds and influence on geothermal activity (Yousefi et al., 2007)

Geochemical: Proximity to altered grounds [m]		
Distance	**Category**	**Score**
Greater than 4000	Least suitable	1
2000-3000	Moderately suitable	2
1000-2000	Suitable	3

Table 3.10: Classification of Hot grounds and influence on geothermal activity (Yousefi et al., 2007)

Geochemical: Proximity to Hot grounds [m]		
Distance	**Category**	**Score**
Greater than 4000	Least suitable	1
2000-3000	Moderately suitable	2
>2000	Most Suitable	3

The aforesaid factors were reclassified and overlain using the union tool in ArcGIS 10.5 to create a suitability map shown in Figure 3.20.

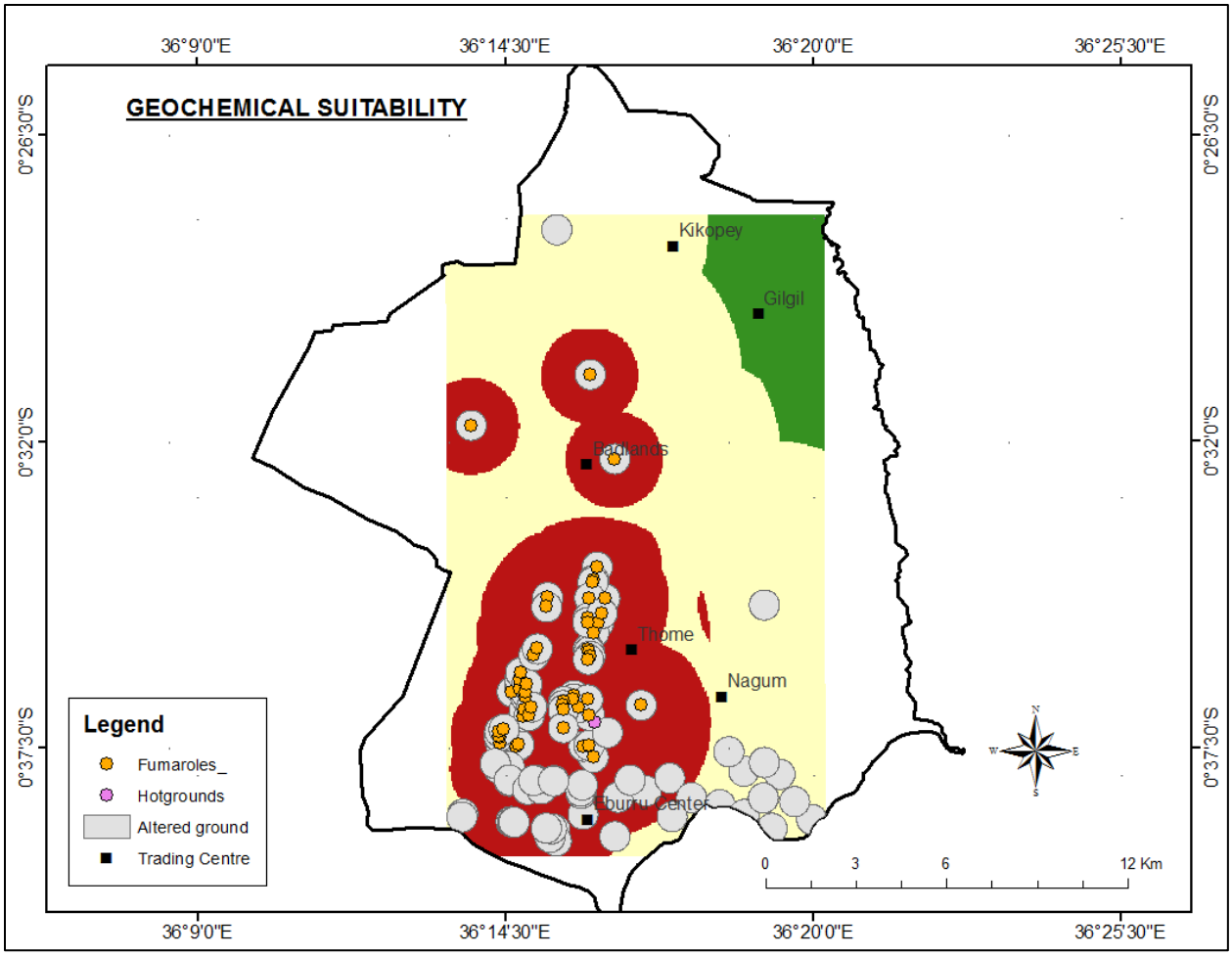

Figure 3.20: Map showing the geochemical Suitability of the study area

3.5.4 Thermal suitability map

A thermal suitability map was developed by merging the satellite land surface temperature data with heat loss survey data. The temperature values were assigned scores based on opinion from the well siting committee survey results as shown in Table 3.11.

Table 3.11: Classification of Temperature and influence on geothermal activity (Yousefi et al., 2007)

Thermal: Surface temperature distribution [°C]		
Temperature range (° C)	**Category**	**Score**
>25	Least suitable	1
25-50	Moderately suitable	2
<50	Most Suitable	3

Using the index overlay function in ArcGIS 10.5, a temperature suitability model was developed as shown in Figure (3.18).

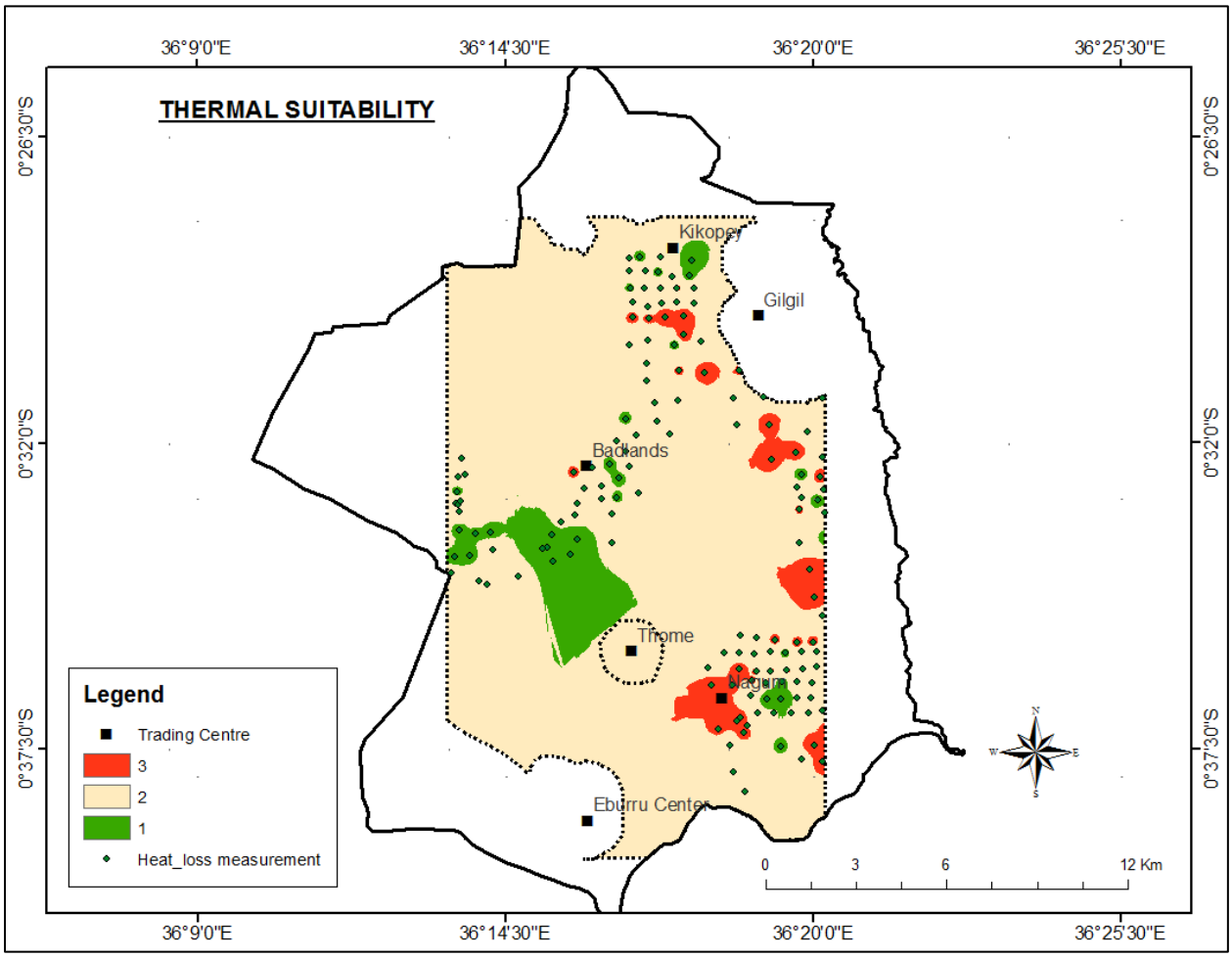

Figure 3.21: Thermal suitability map

Most of the areas in the study area showed moderate suitability to low suitability except areas NW of Thome trading center.

3.5.5 Combined Geothermal suitability map

A combined suitability map (Figure 3.22) was developed by integrating the three geothermal factor layers in using Boolean logic to establish three suitability zones:

i. Most suitable for geothermal power generation
ii. Moderately suitable
iii. Least suitable areas.

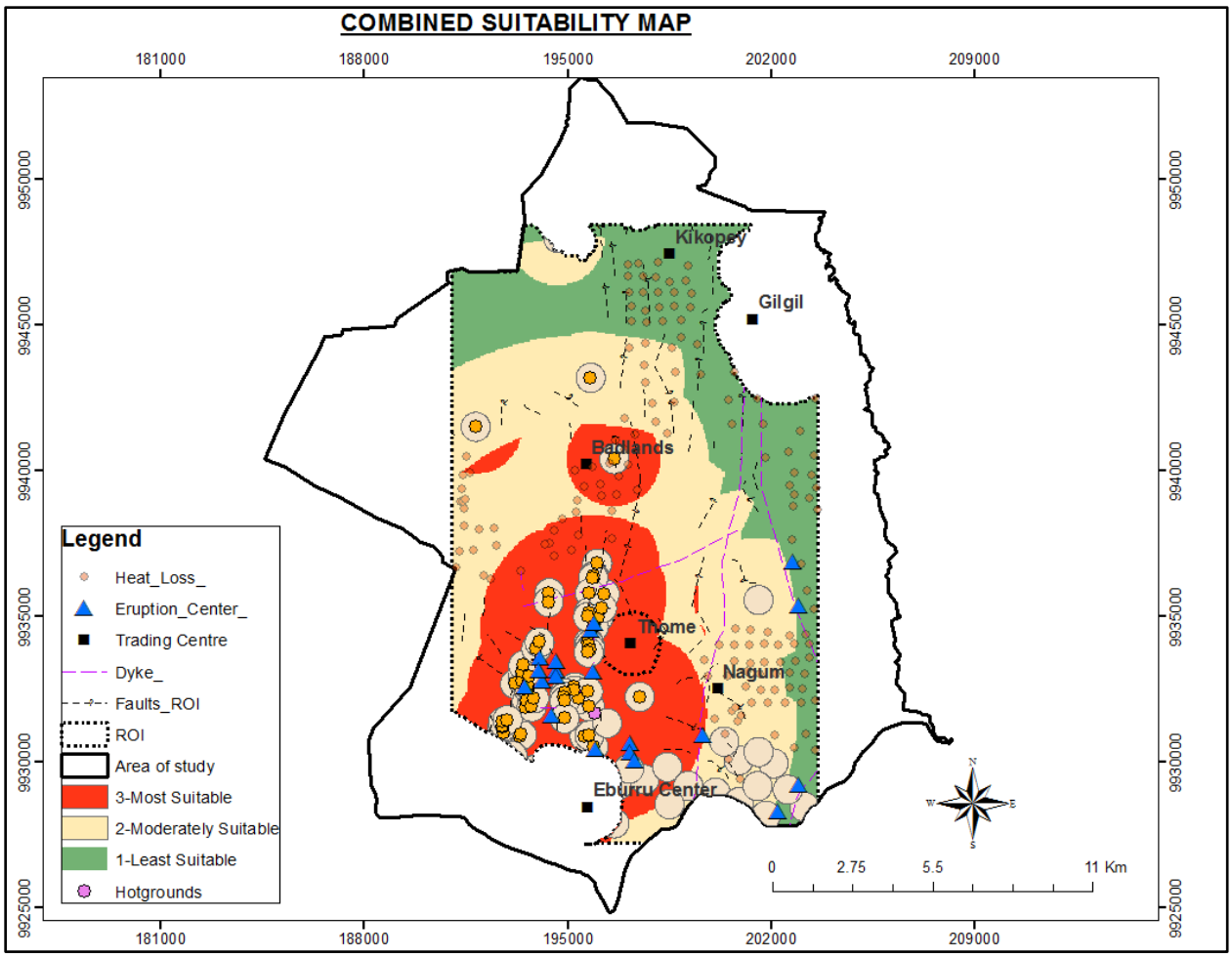

Figure 3.22: Combined suitability map

3.6 The Existing Eburru suitability maps

Two suitability models developed by Varet (2017) and KenGen (2018) were used for comparison. The suitability model was developed by (Varet, 2017) was presented in form of Google Earth image (Figure 3.23). He proposed that siting of geothermal wells be done near phreatic craters. Subsequent sites were identified East, West and Northern parts of Eburru area; mostly targeting the fault orientations. He also proposed an extension of the geothermal field to the Badlands rift axis which lies in the Northern part of the study area.

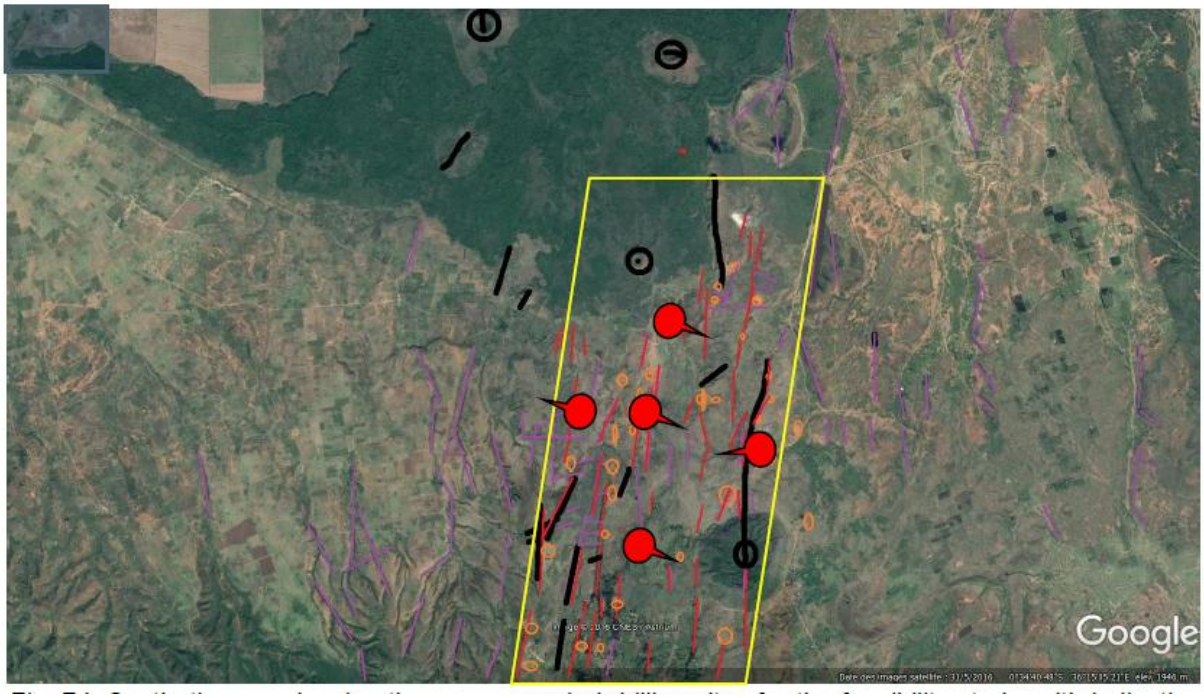

Figure 3.23: Map showing the recommended drilling sites (Varet, 2017)

The suitability map developed by (KENGEN, 2018) identified three prospect areas. The first prospect site was at the Eburru Massif, SE of KenGen's drilled well (EW-01). This suitability map was created using geophysical, resistivity measurements. The second well site was proposed in Thome area. They identified this prospect by characterizing the micro graben system and adjacent rhyolitic dykes. Geochemical features such as high temperature ranging from 86-98°C were also used to develop the suitability model. They proposed a third site near Nagum area at the northern tip of the Waterloo ridge. Resistivity measurements were used to detect anomalous zones extending approximately 6km. They further stated that the area lie on a faulted fissure zone with high geothermal energy potential. These findings were represented in form of 2D map (Figure 3.24).

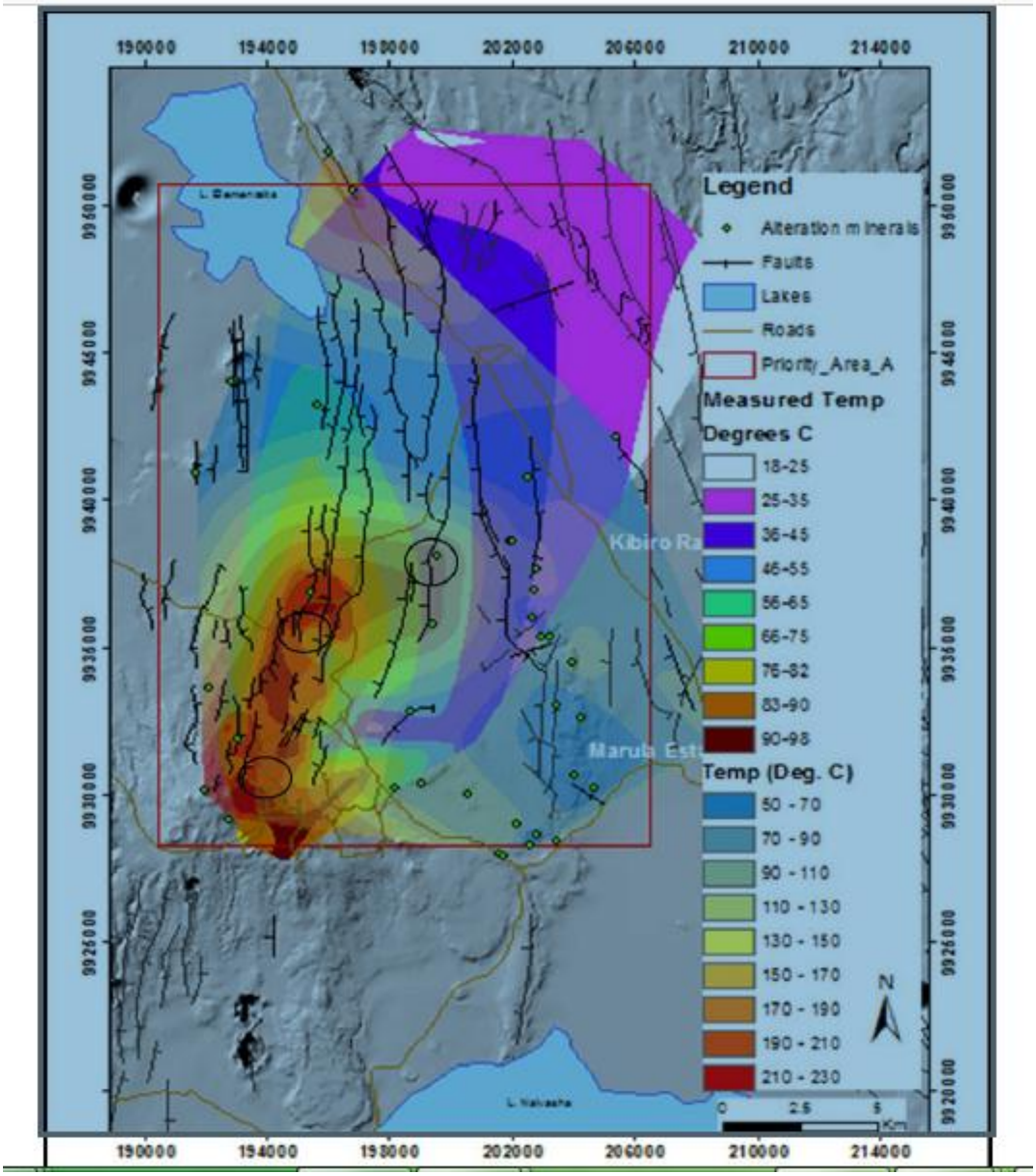

Figure 3.24: Suitability map of the study area (KenGen, 2018).

CHAPTER FOUR

4 RESULTS AND DISCUSSION

4.1 Criteria weights

In pursuit of objective one and two of the study, weighted overlay analysis was done based on the relative influence of the geothermal factors that were discussed in the previous chapters. These results are represented in Table 4.1, 4.2 and 4.3.

Table 4.1: Weighted index table for geological features (User satisfaction survey)

Weighted index Table	
Factor	**% influence**
Faults	40
Eruption Centers	35
Dykes	25

Table 4.2: Weighted index table for geochemical features (User satisfaction survey)

Weighted index Table	
Factor	**% influence**
Fumaroles	40
Altered Grounds	30
Hot grounds	30

Table 4.3: Weighted index table for surface temperature (User specification survey)

Thermal: Surface temperature distribution [°C]	
Temperature range (° C)	**% influence**
>25	15
25-50	35
>50	50

A final weighted index criteria was developed by the aggregating geological, geochemical, and thermal factor maps using a weighted overlay analysis and a multi-class suitability ranking discussed in chapter two and shown in Table 4.4.

Table 4.4: Weighted overlay analysis procedure ((Mayfield, 2016)

Geochemical: Proximity to Hot grounds [m]		
Factor	**% influence**	**Score**
Geological	50	3
Geochemical	30	2
Thermal	20	1

From Table 4.4, the information layers were weighted based on their relative influence in the range of 1 to 3. The weights were assigned in the following order: 3 for geological layers (highest influence), 2 for geochemical (Moderate influence) and 1 (least influence) for thermal layers.

4.2 Final Suitability map

In pursuit of objective three of the study, a final suitability map was developed by integrating the three geothermal factor evidence layers and filtering the restricted areas as shown in Figure 4.1.

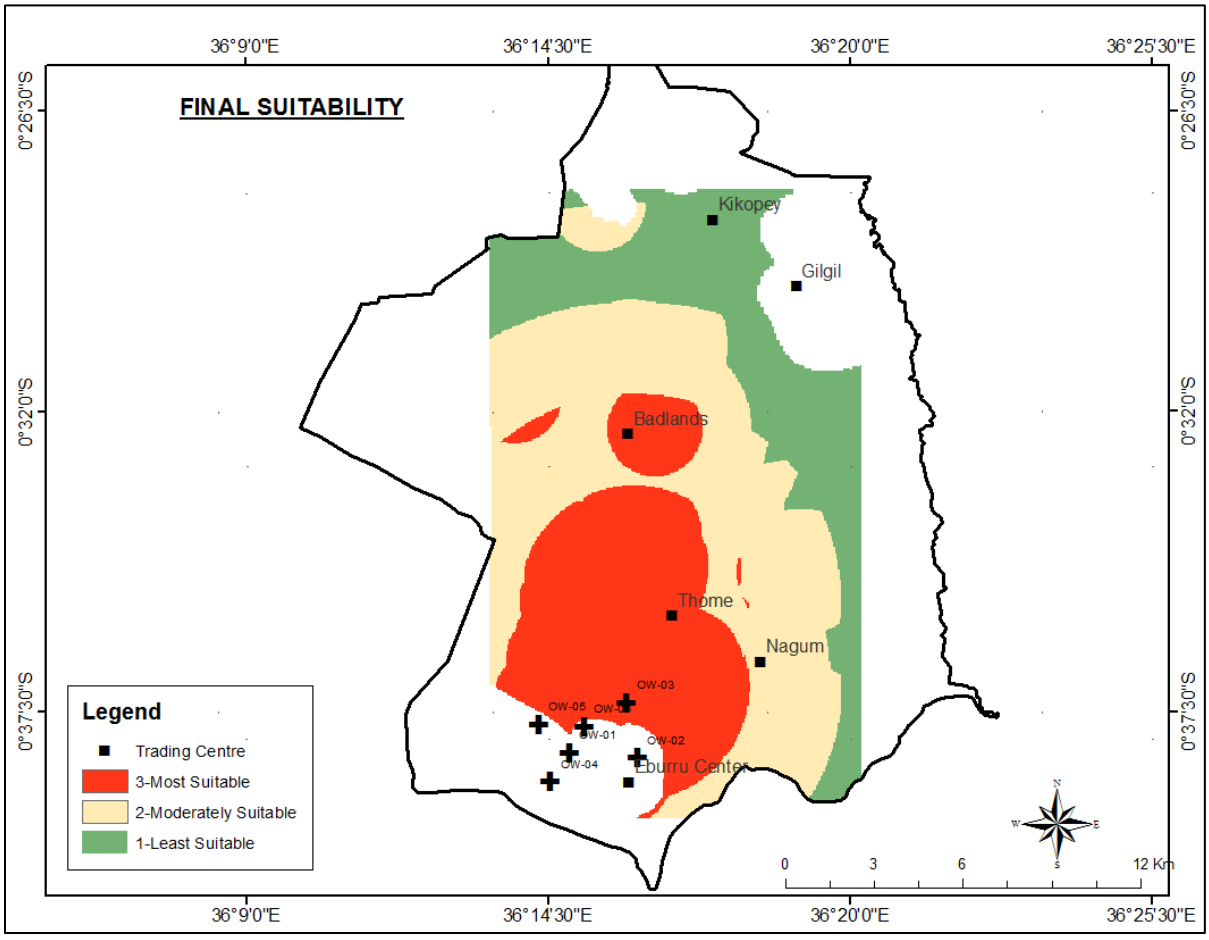

Figure 4.1: Final suitability map of the study area

From the suitability map, areas around Eburru, Thome trading centers and Badlands Rift axis are the most promising sites for geothermal well siting. These areas are flanked by numerous geothermal manifestation features as evidenced by field data. The six wells drilled by KenGen were sited in this area. The Badlands area is also adjacent to the Badlands basaltic flow that postulated to be in near the magmatic heat source located along the Elementaita-Eburru rift axis. Areas that are North of Badlands area, Lake Elementaita buffer area and Nagum have medium geothermal energy potential. The Eastern areas near Gilgil and North Eastern regions near Kikopey trading centers have low potential. The area's suitability classes are presented in Table 4.5.

Table 4.5: Suitable areas for geothermal well siting in the study area

Suitability index	Location
Most suitable	1000m North of Eburru Trading Centre
	Badlands Rift axis (Preferable the Eastern part close to the basaltic lava flow)
Moderately suitable	Thome area
	Nagum area and 250m South of Lake Elementaita
Least Suitable	Areas extending NE and E of the study area close to Gilgil town and Kikopey trading center

The results from the suitability map were statistically computed to establish the area of coverage based on the count of each of the three classes involved in the combined suitability map creation. The percentage suitable areas (after filtering of the constraints), are represented in Table (4.6).

Table 4.6: Area of coverage combined suitability classes

Class	Suitability	% Area	Area (Km^2)
1	Least Suitable	32	95.616
2	Moderately suitable	36	107.468
3	Most suitable	34	101.592

4.3 Comparison between the final geothermal suitability map and existing Eburru suitability map

As per the fourth specific objective of the study, similarities were drawn between the developed suitability map and the aforementioned existing maps done by KenGen (2018) and Varet (2017). The findings are tabulated in Table 4.7.

Table 4.7: Comparison between existing and new suitability map

Suitability model	**Location of geothermal Resource**	**Factors used for model creation**	**Environmental Constraints considered**
Varet (2017)	East, West and Northern parts of Eburru area and the Badlands Rift axis	Satellite imageries, Geological observations	None
KenGen (2018) model	(1.). Eburru massif area, SE of EW-01. (2). Thome area, South of Eburru Centre (3.). Nagum, NE of Eburru area	Geophysical resistivity measurements, Heat loss measurements, geological data, geochemical	Game reserves (Marula conservancy), specific tree species.
Current study	Eburru Massif area, Thome, and Badlands Rift axis	Geological (faults/fractures, dykes, eruption centers), geochemistry (fumaroles, altered grounds, hot grounds), thermal (LST, heat loss surveys)	Riparian (Lake Elementaita), Forest cover, Residential areas

4.3.1 Discussion

It was established that the three suitability maps confirmed the existence of resource in the northern areas near Badlands Rift axis and Thome trading center. The two maps by KENGEN (2018) and the current study confirmed the existence of geothermal resource at the Eburru trading center, near the Eburru massif area.

The eastern regions near Waterloo ridge and Nagum trading centers were classified to be highly suitable as per the findings by KENGEN (2018). This contrasts the current study's findings and Varet (2017) which categorized them as moderate. All suitability maps categorized the North Eastern regions of Gilgil town and Kikopey shopping centers as least suitable. This might be attributed to low relative weights assigned to the geothermal factors and the influence this had in the suitability map creation.

CHAPTER FIVE

5 CONCLUSIONS AND RECOMMENDATIONS

5.1 Conclusion

The criteria weights generated using weighted overlay analysis method for the three geothermal factors confirmed the existence of geothermal energy resource in the study area. The relative influence of each individual geological factor was 40%, 35% and 25% for faults, eruption centers and dykes respectively. As for the geochemical factors, the relative influence of fumaroles, altered grounds and hot grounds was 40%, 30% and 30% respectively. The relative influence of the surface temperature distribution (thermal factor) was 50%, 35% and 15% for the ranges of >50°C, 25-50°C and < 25°C respectively. In general the overall relative influence of the main factors was 50%, 20% and 30% for geological, geochemical and thermal factors respectively.

From the final suitability map, areas near Eburru Trading Center, Thome village (North of study area) and areas near the Badlands rift axis were deemed most suitable for geothermal well site selection. These areas cover about 34% (about 101km^2) of the region of interest. The high geothermal suitability can be attributed to tectonic activities around these zones. Areas near Nagum, village, near the waterloo ridge and south of Lake Elementaita areas were deemed moderately suitable. They covered about 36% (108 km^2) of the area of interest. Finally, the North Eastern (Gilgil, Kikopey centers) and Western parts of the region of interest were considered least suitable. They covered about 95km^2 (30%) of the region of interest. In general, geothermal suitability decreases with increasing distance from surface manifestation feature (geothermal factors) as evidenced by the decrease of potential from Eburru shopping area towards Lake Elementaita and Gilgil area.

Comparisons with existing suitability maps concurs with most of the study's findings. The only differences arose from the recommendations by KENGEN (2018) who confirmed the presence of geothermal resource near Nagum village.

It can therefore be concluded that all the study objectives were achieved. Based on the aforementioned advantages of the study technique, it should therefore be considered in future geothermal resource exploration activities.

5.2 Recommendations

The following are the recommendations based on study findings:

i. Carbon dioxide and radon gases distribution plus geophysical factor criteria be considered for better and more precise suitability model development.

ii. Use higher spatial resolution images (preferably Geoeye-1) to enhance digitization process.

iii. Use sensitivity analysis to validate and assess reliability of the study's findings.

iv. Use the simple additive weighting method to compute the weighted average of preferences based on an arithmetic mean. This will enhance accuracy of the weighting process and improve the overall reliability of the study's findings.

v. Consider performing a 3D multi-criteria analysis by integrating subsurface geothermal well data and surface exploration datasets. This will aid in visualization and projection of subsurface information for more accurate and precise well site selection.

vi. Optimization studies to determine minimum separation distance between proposed adjacent geothermal wells and minimum number of wells in a prospect area.

REFERENCES

Abdullah, A., Nassr, S., & Ghaleeb, A. (2013). Remote Sensing and Geographic Information System for Fault Segments Mapping a Study from Taiz Area, Yemen. *Journal of Geological Research*, 1–16. https://doi.org/s http://dx.doi.org/10.1155/2013/201757

Al-Amri, M. A., & Eldrandaly, K. A. (2014). *A proposed GIS-based decision making framework for tourism development sites selection*. Presented at the The International Arab Conference on Information Technology (ACIT).

Araneo, R. S., & Vergine, C. (2015). Eco-sustainable routing of power lines for the connection of renewable energy plants to the Italian high-voltage grid. *International Journal of Energy and Environmental Engineering*, *6*, 9–19.

Árnason, K., Vilhjálmsson, A. M., & Björnsdóttir, T. (2007). A STUDY OF THE KRAFLA VOLCANO USING GRAVITY, MICRO EARTHQUAKE AND MT DATA. *United Nations University Geothermal Training Program*, 14.

Bjorke, J. K. (2010). *Fluid-rhyolite interaction in geothermal systems, Torfajokull Iceland-secondary surface mineralogy and fluid chemistry upon phase seggregation and fluid mixing* (Thesis). University of Iceland, Reykjavik.

Braddock, M., Biggs, J., Watson, I. M., Hutchison, W., Pyle, D. M., & Mather, T. A. (2017). Satellite observations of fumarole activity at Aluto volcano, Ethiopia: Implications for geothermal monitoring and volcanic hazard. *Journal of Volcanology and Geothermal Research*, *341*, 70–83. https://doi.org/10.1016/j.jvolgeores.2017.05.006

Brandmeier, M., Erasmi, S., Hansen, C., Höweling, A., Nitzsche, K., Ohlendorf, T., … Wörner, G. (2013). Mapping patterns of mineral alteration in volcanic terrains using ASTER data and field spectrometry in Southern Peru. *Journal of South American Earth Sciences*, *48*, 296–314. https://doi.org/10.1016/j.jsames.2013.09.011

Bromley, C. J. S. M. van M., & Graham, D. (2010). Monitoring surface geothermal features using time series of aerial and ground-based photographs. *American Geophysical Union*.

Chander, G., Markham, B. L., & Helder, D. L. (2009). Summary of current radiometric calibration coefficients for Landsat MSS, TM, ETM+, and EO-1 ALI sensors. *REMOTE SENS. ENVIRON*, *113*(5), 893–903. https://dx.doi.org/10.1016/j.rse.2009.01.007

Chasia, A. S. (2014). *Mapping Geological Structures in Western Mutomo, Kitui County: a Remote Sensing Approach* (M.Sc. Thesis). University of Nairobi, Nairobi.

Chaudhry, R. (2008). *Using Multi-Criteria Evaluation to Determine Suitable Sites for Developing Wind Farms in Massachusetts* (p. 16). Worcester, USA,: Clark University.

Ciaccia, G. N., Doni, N., & Fontini, F. (2010). *Auctioning wind power sites when environmental quality matters* (pp. 1734–1740).

Dickson, M. H., & Fanelli, M. (2004). What is geothermal energy? [Internet website]. Retrieved from http://www.geo-exchange.ca/fr/Pdf/Geothermal%20 Energy.pdf,

ERC. (2012). *Geothermal Resources*. Retrieved from https://renewableenergy.go.ke/index.php/content/28

Fargione, J. J., Slaats, M. J., & Olimb, J. (2012). Wind and Wildlife in the Northern great plains: Identifying low-impact areas for wind development. *PLOS ONE*, *7*.

Frutuoso, R. (2015). Mapping hydrothermal gold mineralization using Landsat 8 data. A case of study in Chaves license, Portugal. *University of Porto*, 85.

Glassley, W. E. (2014). *Geothermal Energy: Renewable Energy and the Environment* (2nd ed., Vol. 2). Florida: CRC Press.

Gudni, A., & Hjalti, F. (2012). GEOTHERMAL DRILLING TARGETS AND WELL SITING. *UNU-GTP*, 1–14.

Hannssen, F., Roel, M., & Jiska, van D. (2018). Spatial Multi-Criteria Decision Analysis Tool Suite for Consensus-Based Siting of Renewable Energy Structures. *Journal of Environmental Assessment Policy and Management*, 1–27.

Haselwimmer, C., & Prakash, A. (2013). Thermal Infrared Remote Sensing of Geothermal Systems. In C. Kuenzer & S. Dech (Eds.), *Thermal Infrared Remote Sensing* (Vol. 17, pp. 453–473). https://doi.org/10.1007/978-94-007-6639-6_22

Jacob, F., Petitcolin, F., Schmugge, T., Vermote, E., French, A., & Ogawa, K. (2004). Comparison of land surface emissivity and radiometric temperature derived from MODIS and ASTER sensors. *Remote Sensing of Environment*, *90*(2), 137–152. https://doi.org/10.1016/j.rse.2003.11.015

Jensen, R. J. (2013). *Remote Sensing of the Environment* (2nd ed., Vol. 4th). New Delhi: Dorling Kindresley (india).

KENGEN. (2018). *Geological, Structural and Hydrogeological Mapping of the Eburru-Marulla-Badlands Geothermal Prospect-Phase II* (pp. 1–53) [Internal Report]. Naivasha: Kenya Electricity Generating Company – KenGen.

Kipsang, C. (2015). Cost Model for Geothermal Wells. *World Geothermal Congress 2015*, 1–12. Melbourne: Kenya Electricity Generating Company Limited.

Lillesand, T., Kiefer, W. R., & Chipman, J. (2015). *Remote Sensing and Image Interpretation* (7th ed., Vols. 1–7). Danvers: John Wiley & Sons, Inc.,.

Littlefield, F. E., & Calvin, M. W. (2014). Geothermal exploration using imaging spectrometer data over Fish Lake Valley, Nevada. *Remote Sensing of Environment*, *140*, 509–518.

Macharia, W. M., Gachari, K. M., Kuria, D. N., & Mariita, O. N. (2017). Low cost geothermal energy indicators and exploration methods in Kenya. *Journal of Geography and Regional Planning*, *10*(9), 254–265. https://doi.org/10.5897/JGRP2017.0643

Mayfield, C. J. (2016). *Automating the Classification of Thematic Rasters for Weighted Overlay Analysis in GeoPlanner for ArcGIS* (Msc Thesis). University of Redlands, Carlifonia.

Mia, B., & Fujimitsu, Y. (2012). Mapping hydrothermal altered mineral deposits using Landsat 7 ETM+ image in and around Kuju volcano, Kyushu, Japan. *Journal of Earth System Science*, *121*(4), 1049–1057. https://doi.org/10.1007/s12040-012-0211-9

Mibei, G. (2012). *Status of geothermal exploration and development in Kenya*. Presented at the Short course VIII on exploration for geothermal resources, Naivasha.

Munyiri, S. K. (2016). *Structural mapping of Olkaria Domes geothermal field using geochemical soil gas surveys, remote sensing and GIS* (M.Sc. Thesis). UNU Geothermal Training Programme, Reykjavik.

Mwaura, D. W. (2018). *Exploration and Optimized Siting of Geothermal Wells Using aWeb-Based Spatial Decision Support System: A Case Study of the Olkaria Geothermal Field* (PhD thesis). Technische Universität Berlin, Berlin.

Noorollahi, Y. (2005). *Application of GIS and remote sensing in exploration and environmental management of Námafjall geothermal area, N-Iceland*. United Nations University, Geothermal Training Programme, Reykjavík Iceland.

Noorollahi, Y., Ghasempour, R., & Jalilinasrabady, S. (2015). A GIS Based Integration Method for Geothermal Resources Exploration and Site Selection. *Energy Exploration & Exploitation*, *33*(2), 243–257. https://doi.org/10.1260/0144-5987.33.2.243

Ochieng, L. (2013). OVERVIEW OF GEOTHERMAL SURFACE EXPLORATION METHODS. *UNU-GTP*, 13.

Ólafsson, J. M. (2018). *UAV Geothermal Mapping in Austurengjar* (M.Sc. Thesis, Reykjavík University). Retrieved from https://skemman.is/bitstream/1946/31409/1/J%C3%B3hann%20Mar%20%C3%93lafsson%20Thesis_Final_Version_last1.pdf

Omenda, P. A. (2013). GEOTHERMAL EXPLORATION IN KENYA. *UNU-GTP*, *VIII*, 14.

Omenda, P. A., Onacha, S. A., & Ambuso, J. W. (1993). *Occurence and Distribution of High Temperature Geothermal Systems in Kenya*. 241–246. Retrieved from http://www.geothermal-energy.org/pdf/IGAstandard/NZGW/1993/Omenda.pdf

Onyango, O. O. (2018, June 5). Kenya tops Africa, ninth globally in geothermal rankings. *Daily Nation@nation.Co.Ke*. Retrieved from https://www.nation.co.ke/business/Kenya-tops-Africa--ninth-globally-in-geothermal-rankings/996-4597034-o5iddy/index.html

Pour, A. B., Hashim, M., & van Genderen, J. (2013). Detection of hydrothermal alteration zones in a tropical region using satellite remote sensing data: Bau goldfield, Sarawak, Malaysia. *Ore Geology Reviews*, *54*, 181–196. https://doi.org/10.1016/j.oregeorev.2013.03.010

Rybach, L. (1981). *Geothermal Systems, Conductive Heat Flow, Geothermal Anomalies*. New York: John Wiley & Sons, Inc.,.

Sarpong, D., & Baffoe, P. E. (2016). Selecting Suitable Sites for Wind Energy Development in Ghana. *Ghana Mining Journal*, *16*(1), 8–20. http://dx.doi.org/10.4314/gmj.v16i1.2

Schmugge, T., French, A., Ritchie, J., Rango, A., & Pelgrum, H. (2002). Temperature and emissivity separation from multispectral thermal infrared observations. *Remote Sensing of Environment*, *79*, 189– 198.

Shako, L., & Wamalwa, A. (2014). GIS Applications in Heat Source Mapping in Menengai Geothermal Field. *Proceedings 5 Th African Rift Geothermal Conference 2014 (ARGeo-C5)*, 1–14. Arusha: ArGeo.

Simao, A., Densham, P. J., & Haklay, M. M. (2009). Web-based GIS for collaborative planning and public participation: An application to the strategic planning of wind farm sites. *Journal of Environmental Management*, *90*, 2027–2040.

van der Meer, F., Hecker, C., van Ruitenbeek, F., van der Werff, H., de Wijkerslooth, C., & Wechsler, C. (2014). Geologic remote sensing for geothermal exploration: A review. *International Journal of Applied Earth Observation and Geoinformation*, *33*, 255–269. https://doi.org/10.1016/j.jag.2014.05.007

Varet, J. (2017). *Report on Badlands (West from Gilgil) structural geology, volcanology and igneous rocks petrology allowing for a first geothermal conceptual model* (pp. 1–49). Nyeri: Dedan Kimathi University of Technology.

Varghese, J. (2016). *Detecting the effect of Soil Moisture and Hot spot size on geothermal anomalies via Remote sensing techniques* (M.Sc. Thesis). University of Twente, Enschede.

Velador, M. J., Omenda, P. A., & Anthony, Y. E. (2003). An integrated Mapping and Remote Sensing Investigation of the Structural control for Fumarole location in the Eburru Volcanic Complex, Kenya Rift. *Geothermal Resource Council*, *27*, 12–15.

Yetkin, E. (2003). *Alteration Mapping by Remote Sensing: Application to the Hasandag-Melendiz Volcanic Complex* (M.Sc. Thesis). Middle East Technical University, Ankara.

Yousefi, H., Ehara, S., & Noorollahi, Y. (2007). Geothermal Potential Site Selection using GIS in Iran. *Geothermal Reservoir Engineering*, *32*, 9.

Zhong, S., Zhang, Y., Chen, Y., & Wu, D. (2017). Combining Component Substitution and Multiresolution Analysis: A Novel Generalized BDSD Pansharpening Algorithm. *IEEE JOURNAL OF SELECTED TOPICS IN APPLIED EARTH OBSERVATIONS AND REMOTE SENSING*, *10*(6), 2867–2875. https://doi.org/10.1109/JSTARS.2017.2697445

Appendix 1: Heat Loss survey measurements of the study area

Point	Easting	Northing	Elevation (m)	Temp (^{0}C) at 50cm	Temp (^{0}C) at 100cm	Temp (^{0}C) at 150cm
SP1	200927.5	9929417	2097	24.8	24.8	25.3
SP2	200543.3	9930082	2155	27.7	28	27
SP3	200402.4	9930970	2210	30.2	28.5	26.2
SP4	200047.1	9931506	2240	23.2	24.3	27.6
SP5	200627.6	9931771	2199	22.8	22.8	22.5
SP6	200859.7	9931389	2184	21.9	23.1	25.9
SP7	200974.4	9931606	2177	24.3	26.5	28.8
SP8	200750.1	9931880	2205	21.4	23.4	24.1
SP9	201116.6	9932600	2069	28.8	26.7	27.3
SP10	201336.4	9932045	2093	30.1	30.6	28.6
SP11	201872.5	9932026	2067	29.8	28.1	28.8
SP12	202463.1	9932038	2055	29.8	28.9	28
SP13	203032.1	9932033	2080	27.2	26.6	26.8
SP14	203087.2	9932525	2077	26.9	26.9	27.9
SP15	203142.8	9933052	2082	29.6	29.5	31.3
SP16	202648.1	9933058	2061	28.3	26.8	27.5
SP17	202650.1	9932548	2051	30.3	28.7	29.1
SP18	202110.5	9932495	2047	34.1	30.4	28.6
SP19	202138.3	9933054	2049	32.7	30.5	27.2
SP20	201616.1	9933019	2028	31.2	31.2	26.7
SP21	201625.2	9932489	2060	32.2	28.8	27
SP22	201160.5	9933105	2044	23.2	23.5	22
SP23	200499.1	9932961	2059	22.8	22.6	22.3
SP24	199798.2	9932955	2113	21.4	22.2	23.5
SP25	200730.5	9933480	2058	20.2	21.6	22.6
SP26	201280.9	9933411	2048	23.6	23.5	25.8
SP27	201765.6	9933414	2058	23	25.7	22.4
SP28	202306.2	9933447	2070	22.9	23	26.5
SP29	202826.6	9933484	2076	25.3	24.4	25.6
SP30	203296.2	9933576	2088	25.6	24.7	25.5
SP31	203295.6	9934077	2092	25	24.4	23.7
SP32	202778.2	9934065	2092	24.2	29.9	29
SP33	202252.3	9934018	2088	33	31	30.3
SP34	201747.5	9934082	2080	28.6	31	27.5
SP35	201225.7	9934008	2063	28.7	28.8	27.2
SP36	200723.2	9934019	2072	29	27.2	26.1
SP37	200213.3	9934018	2077	29.2	26.1	27
SP38	199699.9	9933530	2133	27.2	27.8	26

Point	Easting	Northing	Elevation (m)	Temp (^{0}C) at 50cm	Temp (^{0}C) at 100cm	Temp (^{0}C) at 150cm
SP39	200750.1	9934601	2077	29.4	27.5	26.3
SP40	201289.3	9934546	2070	28.6	27.8	26.5
SP41	201895.4	9934450	2091	22.1	23.4	26.8
SP42	202625.2	9934363	2087	23.2	23.7	26.8
SP43	203194.2	9934390	2071	23.4	24.5	24
SP44	203495.9	9932107	2164	24.3	24.2	23.5
SP45	203566	9931524	2138	23.5	23.8	26.7
SP46	203984.3	9931560	2105	24.5	24	24.6
SP47	204632.8	9931131	1958	27.4	29.7	31
SP48	204274.3	9930918	2025	28.7	27.3	28.4
SP49	205287.3	9931041	1919	27.8	24.6	22.5
SP50	205628.2	9931090	1899	24.5	24.5	23.5
SP51	205467.5	9931549	1912	22.4	22.3	23.2
SP52	204957.7	9931538	1937	24.1	23.3	23
SP53	206009.8	9931625	1899	23.4	23.9	25.2
SP54	206382.3	9931900	1903	25	25	25
SP55	206252	9932462	1912	25.2	25.2	25.4
SP56	205920.1	9932146	1908	25	25	25.2
SP57	205262.2	9931911	1934	25.6	26.5	27.8
SP58	204622.5	9931666	1976	25.7	27	26.9
SP59	207038	9931806	1898	28.3	27.7	27.1
SP60	207005.2	9932350	1910	29.2	27.5	26.5
SP61	207000.2	9932882	1918	28.2	28.6	27.4
SP62	206828.9	9933316	1918	29.1	28.1	28.1
SP63	206504.8	9932969	1913	30.2	30.2	29.1
SP64	206389	9933420	1921	31.2	30.3	27.3
SP65	206491.3	9934889	1924	29.5	28.1	27.6
SP66	205782.4	9932933	1923	28.3	26.7	27.4
SP67	205911.3	9933450	1926	31.3	29.8	28.5
SP68	205295.9	9933145	1963.006	20.9	23.5	27.2
SP69	205197.4	9932634	1975.46	25.7	27.7	31.2
SP70	204765.2	9932354	2003.69	30.8	28.9	25.1
SP71	204550.9	9932804	2019.54	25.4	26.2	27.2
SP72	204180.6	9933154	2078.4	28	24.9	26.8
SP73	204009	9934183	2166.8	26.7	24.2	25.6
SP74	203648.6	9932756	2106.05	27.7	24.7	26.2
SP75	204042.5	9933940	2009.29	27.1	24.6	27
SP76	205029.7	9934968	1928.28	29.3	24.2	24.3
SP77	206814.9	9934623	1935.11	25.4	23.4	22.5
SP78	205059.9	9927987	1892.73	23.3	23.8	24.5

Point	Easting	Northing	Elevation (m)	Temp (^{0}C) at 50cm	Temp (^{0}C) at 100cm	Temp (^{0}C) at 150cm
SP79	205037.2	9928644	1895.12	22.6	23.1	23.5
SP80	205819.8	9929300	1894.54	25.2	24	23.6
SP81	204336.5	9927969	1899.87	24.6	22.3	22.4
SP82	204075.8	9928280	1934.86	23.8	24.1	23.6
SP83	203768.9	9928911	1924.49	23.1	24.6	24.6
SP84	203494.6	9930420	2095.05	22.7	28.6	28.6
SP85	203199.3	9930970	2096.99	19.7	24	24
SP86	202115.7	9930934	2088.38	31.9	25	27
SP87	202809.6	9930496	2057.13	26.6	25.4	25.8
SP88	204821	9930204	1989.85	24.3	23.2	23.4
SP89	204733.3	9929978	1897.83	24.3	23.2	23.4
SP90	205690.9	9935652	1934.799	20.6	22.5	24.2
SP91	203208.1	9935883	2025.53	22.6	24.4	24.8
SP92	203479.8	9935246	2029.3	25	22.5	22.2
SP93	204162.4	9934794	1974.06	26	24	24.1
SP94	204478.1	9935481	1931.31	27.5	24.8	24.8
SP95	205709.5	9937058	1932.85	26.6	24.4	24.7
SP96	204164.5	9937087	1930.13	18.1	22.1	22.2
SP97	203045.7	9936790	1998.15	20.8	21.7	25.2
SP98	202709.3	9937660	2009.45	26.1	25	24.7
SP99	203588.8	9937850	1955.93	32.7	24.7	25.7
SP100	205033.8	9937793	1937.75	30.3	23.9	23.9
SP101	204580.9	9938541	1944.565	24.1	26.7	27.1
SP102	203566.6	9938660	1958.343	25.5	25.5	23
SP103	202731.1	9938790	2036.93	23.1	24.5	24.8
SP104	202629.3	9939503	2019.06	28.7	28.9	30.5
SP105	203525.7	9939441	1969.08	24.2	23.3	24.8
SP106	204494.2	9939464	1948.79	27.9	29.9	30
SP107	204526.9	9940480	1953.3	28.3	28.5	28.3
SP108	203481.9	9940523	1974.45	27	26	24.4
SP109	202609.5	9940653	2020.44	21.6	23.1	23.8
SP110	201801.3	9940456	2048.13	21.6	22.4	23
SP111	204516.4	9939528	2049.16	21.9	23.4	26.1
SP112	201723	9941595	2031.87	23.2	22.9	25.8
SP113	201527.2	9942503	2037.76	25.3	25.5	26.9
SP114	202466.5	9942491	1995.78	25.1	23.5	25.5
SP115	202998	9941380	1981.56	28.6	24.3	23.8
SP116	203611.7	9941541	1973.3	28.3	24.4	24.9
SP117	203493.6	9942485	1981.95	26.6	23.6	24.3
SP118	203224.3	9943538	1988.52	21.9	24	26.5

Appendix 2: Location of Sampled wells

(**Datum**; Arc 1960, **Units**: Meters, **Projection**: Transverse Mercator)

Well	**Eastings**	**Northings**	**elevation (m)**	**drilled-depth (m)**
OW-05	192650.902	9930427.62	2626.77	2217.5
OW-02	196002.56	9929300.82	2476	2786
OW-03	195632.08	9931161.78	2419.9	2596
OW-04	193052.52	9928494.157	2574.5	2464
OW-01	193680.8	9929479.1	2583.2	2467
OW-06	194177.923	9930355.899	2604.9	2481

Appendix 3: Fumarole temperatures

Longitude	Latitude	Temp (^{o}C)
36.24274	-0.63487	97
36.27124	-0.58029	94.9
36.25418	-0.57998	91
36.25391	-0.58282	83.7
36.24493	-0.62456	78
36.24561	-0.62401	77.8
36.24015	-0.6235	56.07
36.23987	-0.62186	66.4
36.2397	-0.62145	67.55
36.23986	-0.62005	84.33
36.24359	-0.60821	58.48
36.24598	-0.60723	72.03
36.24584	-0.6045	83.13
36.2461	-0.60246	80
36.24697	-0.61556	87.2

Appendix 3: User Requirement Analysis

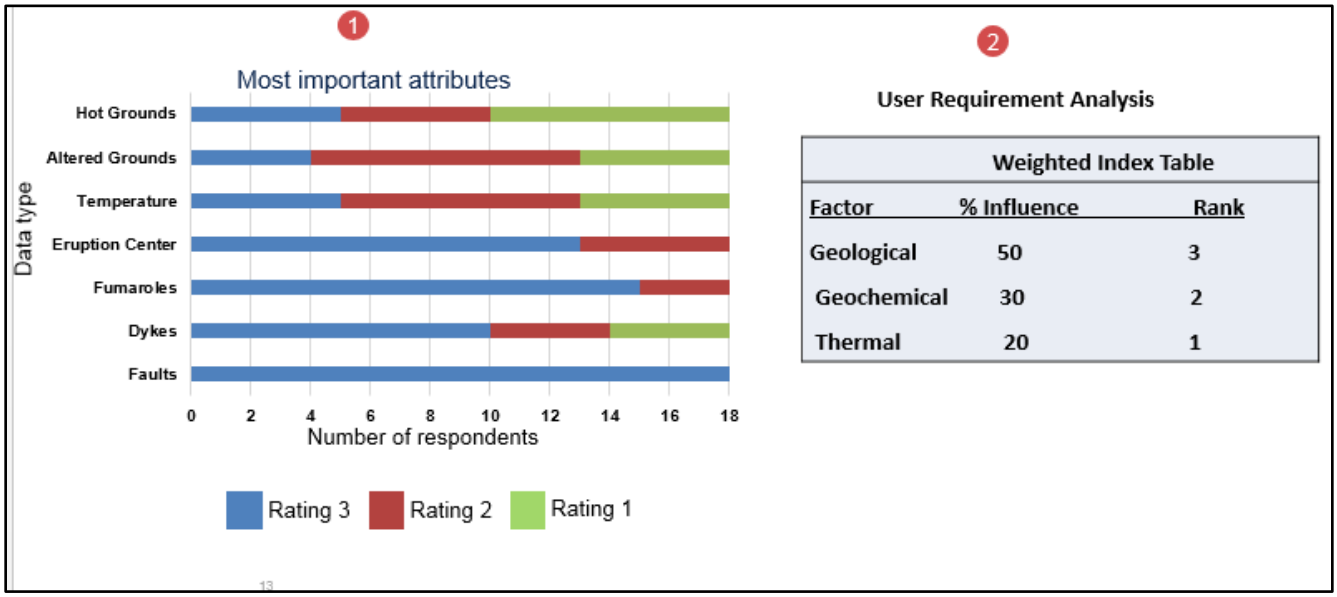

2

User Requirement Analysis

Weighted Index Table		
Factor	% Influence	Rank
Geological	50	3
Geochemical	30	2
Thermal	20	1